AD_____

Award Number: DAMD17-99-1-9564 Volume III

TITLE: Role of Angiogenesis in the Etiology and Prevention of Ovarian Cancer

III: Rational Antiangiogenic Peptide Design-Effect on Ovarian Cancer Growth

PRINCIPAL INVESTIGATOR: Sundaram Ramakrishnan, Ph.D.

CONTRACTING ORGANIZATION: University of Minnesota
Minneapolis, MN 55455-2070

REPORT DATE: October 2003

TYPE OF REPORT: Annual

PREPARED FOR: U.S. Army Medical Research and Materiel Command
Fort Detrick, Maryland 21702-5012

REPORT DOCUMENTATION PAGE

Form Approved OMB No. 074-0188

1. AGENCY USE ONLY (Leave blank)	2. REPORT DATE	3. REPORT TYPE AND DATES COVERED
	October 2003	Annual (1 Oct 2002 - 30 Sep 2003)

4. TITLE AND SUBTITLE
Role of Angiogenesis in the Etiology and Prevention of Ovarian Cancer
III: Rational Antiangiogenic Peptide Design-Effect on Ovarian Cancer Growth

5. FUNDING NUMBERS
DAMD17-99-1-9564

6. AUTHOR(S)
Sundaram Ramakrishnan, Ph.D.

7. PERFORMING ORGANIZATION NAME(S) AND ADDRESS(ES)
University of Minnesota
Minneapolis, MN 55455-2070

E-Mail: sunda001@tc.umn.edu

8. PERFORMING ORGANIZATION REPORT NUMBER

9. SPONSORING / MONITORING AGENCY NAME(S) AND ADDRESS(ES)
U.S. Army Medical Research and Materiel Command
Fort Detrick, Maryland 21702-5012

10. SPONSORING / MONITORING AGENCY REPORT NUMBER

11. SUPPLEMENTARY NOTES
This is Volume III of IV

12a. DISTRIBUTION / AVAILABILITY STATEMENT
Approved for Public Release; Distribution Unlimited

12b. DISTRIBUTION CODE

13. ABSTRACT (Maximum 200 Words)

The purpose of this project to evaluate de novo synthesis of a short polypeptides, which is capable of inhibiting tumor angiogenesis. As tumor growth in general and ovarian cancer in particular is associated with angiogenesis, the synthetic peptide can be used to inhibit growth and peritoneal seeding of ovarian cancer.

14. SUBJECT TERMS
Ovarian Cancer

15. NUMBER OF PAGES
49

16. PRICE CODE

17. SECURITY CLASSIFICATION OF REPORT	18. SECURITY CLASSIFICATION OF THIS PAGE	19. SECURITY CLASSIFICATION OF ABSTRACT	20. LIMITATION OF ABSTRACT
Unclassified	Unclassified	Unclassified	Unlimited

Table of Contents

Annual report for project 3 – October 2002- September 2003
'Rational anti-angiogenic peptide design – effect on ovarian cancer growth'
K.H. Mayo, PI.

INTRODUCTION

The use of agents that can inhibit angiogenesis, particularly in anti-tumor research has indicated that anti-angiogenic therapy can be a promising therapeutic modality in the future. Most anti-angiogenic agents have been discovered by identifying endogenous molecules, primarily proteins, that inhibit EC growth. Some of these angiostatic compounds are currently in various phases of clinical cancer trials (http://cancertrials.nci.nih.gov). Although a number of compounds have shown promise in the clinic, no major breakthroughs have been reported using anti-angiogenic agents as stand-alone therapy. This underscores the need for more and better angiostatic compounds for use as stand-alone treatment or in combination with conventional therapies.

Recently, we reported the design of the anginex peptide (also know as ßpep25), a cytokine-like ß-sheet-forming peptide 33mer, which is a potent inhibitor of angiogenesis and tumor growth. Anginex is more effective at inhibiting EC growth than platelet factor-4 and several other well-known angiogenesis inhibitors such as angiostatin, endostatin, AGM-1470 and thrombospondin-1.

BODY

Hypothesis: Anginex (ßpep25) and its designed analogs can be used to abrogate tumor growth *in vivo* and potentiate the action of chemotherapy or radiation, making use of lower, less toxic, doses of either conventional modalities.

The objectives are to perform *in vitro* and tumor model studies in mice using MA148 ovarian cancer cell line in the absence and presence of either chemo-therapeutic agents or radiation. Studies will be performed to elucidate the essential amino acids of the peptide and by modifying the amino acid sequence, its own efficacy will by tried to be improved. Given the angiostatic potential of anginex and its analogs, the overall aim of this research is to develop anginex or an analog into an anti-tumor therapeutic agent against ovarian cancer.

Relevance to Ovarian Cancer: The tumor model studies mentioned above will be performed using an ovarian cancer cell line, MA148. In this regard, studies will be performed to specifically assess the efficacy of treatment of the peptide and its analogs on ovarian carcinoma.

Methology and Design:

Specific Aim 1: define structure-activity relationships in anginex and design new, more potent ßpep sequences. The ßpep-25 (anginex) sequence will be modified by substituting individual amino acid residues and by analine scanning. Walkthrough peptides will also be generated. Peptides will then be screened for various *in vitro* bioactivities relating to angiostatic potential: endothelial cell (EC) proliferation and collagen gel based tube formation assay. Proper folding of peptides will be assessed by using CD and NMR in order to

differentiate direct and indirect (conformational) effects. The initial round of amino acid substitutions will naturally lead into multiple substitutions and designing in conformational constraints (rationally placed S-S bond(s) or specific turn sequences). Designing and bioassying will be applied iteratively with the intent of improving angiostatic potential.

Results for Aim 1 in year 4: Already in the first 3 years, alanine scanning and walkthrough ßpep-25 peptides were synthesized and analyzed in *in vitro* assays, and structure-function relationships were derived. After identifying the key residues for the activity, all lying on the same surface of the folded peptide, a series of partly non-peptidic mimetics were designed. This series uses a dibenzofuran (DBF) scaffold onto which are covalently attached short, key amino acid sequences derived from anginex. Recently, we provide evidence that ß-sheet is in fact the bioactive conformation of anginex, by using a series of double-cysteine disulfide-bridged analogs CD and NMR spectral analysis of the analogs indicate formation of ß-sheet conformation. As long as placement of disulfide bonds preserved the ß-strand alignment as in the proposed bioactive conformation, bioactivities were preserved.

Specific Aim 2: elucidate the molar mechanism of action of anginex by which angiostatic effects are mediated. This includes identifying the angiostatic pathway, the receptor(s) involved, and the internalization pathway.

Results for Aim 2 in year 4: From former years, we knew that essentials of the molecular mechanism of anti-angiogenic action of anginex. The peptide interacts with a receptor, CD36, on the surface of EC, becomes internalized and triggers the apoptotic cascade. This process is specific for angiogenically-activated EC where CD36 is upregulated, and does not affect resting EC or other cell types. This year, we discovered that anginex may also be interacting with α_2-integrins. The peptides analogs, although highly cytostatic, do not induce apoptosis applying the same mechanism as anginex. A clear understanding of the molecular mechanism of either anginex or its analogs is still in its infancy.

Specific Aim 3: study effectively to inhibit angiogenesis and tumor growth *in vivo.* For this aim, we have focussed on performing nude mouse tumor growth models. In these studies, the ovarian cancer cell line MA148 will be used. In these models, all pre-cinical research can be performed to prepare the research line for phase I clinical trials. Pharmacokinetics and tissue distribution of peptides in animals will then be studied with the use of anti-peptide mAbs, polyclonals and mass spectrometry.

Results for Aim 3 in year 4: The ovarian cancer cell line MA148 has been used in nude mice tumor studies with anginex and its analogs. For these studies, MA148 cancer cells have been injected SC into the hind flank of nude mice and tumors have been allowed to establish prior to administrating the drug. At the optimal dose 10 mg/kg over a 4-week period, tumor size was reduced by about 70%, somewhat greater than that of angiostatin (well-know angiogenesis inhibitor). In this model, one of the analogs, 6DBF7 (also known as CF8) functioned better than parent peptide anginex by reducing tumor volume to about 90% at the same dose. Apparently, this novel design, holding on to the bioactive conformation (ß-sheet), improved the bioavailablity of the pharmaceutic.

Specific Aim 4: investigate combined angiogenesis and chemotherapy *in vivo.* Additional studies will be performed to investigate whether conventional chemotherapy can be improved by co-administration with anti-angiogenic ßpep peptides.

Results for Aim 4 in year 4: Using the ovarian cancer mouse model (MA148) as described above, we were able to show that when anginex (10 mg/kg) was combined with a sub-optimal dose of carboplatin (32.5 mg/kg), tumors regressed to an impalpable state in all the mice. Carboplatin was chosen because it is the leading chemotherapeutic against ovarian carcinoma used in humans. However, these tumors remained undetectable until at least one week after termination of the treatment, after which tumors re-established themselves, indicating continued presence of microscopic disease, which was unresponsive to carboplatin and apparently independent of angiogenesis. In different experiments using the same set-up we combined anginex with chemotherapeutic paclitaxel which not resulted in a synergistic effect when the treatments were combined. Presently we are combining anginex (10 mg/kg) in the ovarian mouse model with a sub-optimal dose of radiation (5 Gy once a week), and tumors regressed to an impalpable state similar to the combination of anginex and carboplatin. Using a syngeneic breast tumor mouse model anginex inhibited the carcinoma growth by about 40% as monotherapy and the combination of anginex with radiation (single dose of 25 Gy) resulted in a significant improvement in survival and complete responses in 60% of the mice.

KEY RESEARCH ACCOMPLISHMENTS

- anginex inhibits the growth of ovarian cancer by about 70%
- using information derived from structural activity assays, functional key residues were identified. In addition, we identified that ß-strand alignment is the bioactive conformation, which was applied in the design of the series of partial non-peptide mimetics. The most efficacious of these analogs is 6DF7.
- 6DBF7 inhibits the growth of ovarian tumors in athymic mice by about 90%, an improvement over anginex.
- when anginex treatment is combined with a sub-optimal dose of carboplatin or radiation in the ovarian mouse model complete tumor regressions are noticeable.

REPORTABLE OUTCOMES

Besides the previous published papers the following have been published this year:

1. Dings RP, Arroyo MM, Lockwood NA, Van Eijk LI, Haseman JR, Griffioen AW, Mayo KH. beta-sheet is the bioactive conformation of the anti-angiogenic anginex peptide. Biochem J 2003;23:281-88.
2. Dings RP, van der Schaft DW, Hargittai B, Haseman J, Griffioen AW, Mayo KH. Anti-tumor activity of the novel angiogenesis inhibitor anginex. Cancer Lett 2003;194:55-66.
3. Dings RP, Yokoyama Y, Ramakrishnan S, Griffioen AW, Mayo KH. The designed angiostatic peptide anginex synergistically improves chemotherapy and antiangiogenesis therapy with angiostatin. Cancer Res 2003;63:382-5.
4. Dings RPM, Nesmelova I, Griffioen AW, Mayo KH. Discovery and development of anti-angiogenic peptides: a structural link. Angiogenesis 2003; *in press.*
5. Mayo KH, Dings RPM, Flader C, Nesmelova I, Hargittai B, Van der Schaft DW, Van Eijk LI, Walek D, Haseman J, Hoye TR, Griffioen AW. Design of a partial-peptide mimetic of anginex with antiangiogenic and anticancer activity. J Biol Chem 2003;*in press.*

CONCLUSIONS

Anginex (ßpep25), and the next generation analog 6DBF7, are effective anti-angiogenic, anti-tumor agents with reasonable high potential for effectivity against ovarian carcinoma in humans especially when applied in combination with the conventional ovarian chemotherapeutic carboplatin.

REFRENCES

None

APPENDICES

Papers listed *in press* under 'Reportable Outcomes'.

Biochem. J. (2003) **373**, 281–288 (Printed in Great Britain)

β-Sheet is the bioactive conformation of the anti-angiogenic anginex peptide

Ruud P. M. DINGS*†, Monica M. ARROYO*, Nathan A. LOCKWOOD‡, Loes I. VAN EIJK†, Judy R. HASEMAN*, Arjan W. GRIFFIOEN† and Kevin H. MAYO*[1]

*Department of Biochemistry, Molecular Biology and Biophysics, University of Minnesota Health Science Center, 6-155 Jackson Hall, 321 Church Street, Minneapolis, MN 55455, U.S.A., †Tumor Angiogenesis Laboratory, Department of Internal Medicine, University of Maastricht, University Hospital Maastricht, P.O. Box 5800, 6202 AZ Maastricht, The Netherlands, and ‡Department of Chemical Engineering and Materials Science, University of Minnesota Health Science Center, 6-155 Jackson Hall, 321 Church Street, Minneapolis, MN 55455, U.S.A.

Anginex is a designed peptide 33mer that functions as a cytokine-like agent to inhibit angiogenesis. Although this short linear peptide has been shown by NMR and CD to form a nascent β-sheet conformation in solution, the actual bioactive structure formed upon binding to its receptor on the surface of endothelial cells could be quite different. By using a series of double-cysteine disulphide-bridged analogues, we provide evidence in the present study that the β-sheet is in fact the bioactive conformation of anginex. CD and NMR spectral analysis of the analogues indicate formation of a β-sheet conformation. Three functional assays, endothelial cell proliferation, apoptosis and *in vitro* angiogenesis, were performed on all analogues. As long as the placement of disulphide bonds preserved the β-strand alignment, as in the proposed bioactive conformation, bioactivities were preserved. Knowledge of the bioactive conformation of anginex will aid in the design of smaller molecule mimetics of this potent anti-angiogenic peptide.

Key words: apoptosis, disulphides, endothelial cell proliferation, NMR, peptide, structure.

INTRODUCTION

Angiogenesis, the formation of new blood vessels out of pre-existing capillaries, is pivotal to a broad array of biological functions, ranging from normal processes like embryogenesis and wound healing to abnormal processes such as tumour growth, arthritis, restenosis and diabetic retinopathy [1,2]. The use of agents that can inhibit angiogenesis *in vitro* and *in vivo*, particularly in anti-tumour research, has indicated that anti-angiogenic therapy can be a therapeutic modality in the future. Most anti-angiogenic agents have been discovered by identifying endogenous molecules, primarily proteins, which inhibit endothelial cell (EC) growth. This traditional approach has produced a number of anti-angiogenics, such as platelet factor-4 (PF4) [3], thrombospondin-1 [4], angiostatin [5], endostatin [6] and bactericidal-permeability increasing (BPI) protein [7].

Recently, we have reported [8,9] the anti-angiogenic activity of a novel peptide 33mer (βpep-25 or anginex). Anginex belongs to a family of homologous βpep peptides that were designed by using basic folding principles and incorporating short sequences from the β-sheet domains of α-chemokines and BPI protein [10]. All βpep peptides form β-sheets to varying degrees and can self-associate in solution as dimers and tetramers [9,10]. A high-resolution NMR structure of tetrameric βpep-4 demonstrated that its monomer subunits are folded into an amphipathic three-stranded anti-parallel β-sheet motif [11]. Two types of six-stranded anti-parallel β-sheet dimers can form and these dimers associate via their hydrophobic faces into tetramers. Although a high-resolution structure of anginex (βpep-25) could not be determined by using NMR because of aggregate exchange resonance broadening, CD and NMR studies [8,9] indicate that anginex also folds primarily into tetrameric β-sheet sandwiches at millimolar concentrations. At concentrations in the micromolar range and lower, however, anginex exists in solution primarily in the monomer state and is composed of a relatively broad distribution of conformations with considerable random coil and some β-sheet character [12]. Therefore, at the micromolar concentrations used in *in vitro* bioassays and *in vivo* animal studies demonstrating the anti-angiogenic [8,9] and anti-tumour [13–15] potency of the peptide, anginex is mostly a random coil monomer. Therefore the bioactive structure of anginex, which is selected from this rather broad conformational distribution, remains unclear.

The aim of the present study was to test the hypothesis that the bioactive conformation of anginex (βpep-25) is a β-sheet with the same strand alignment as in the NMR-derived structure of homologous βpep-4 (see Figure 1) [11]. To accomplish this, a series of disulphide-linked peptide analogues of anginex were made. By comparing activities from all 30 members of the βpep library, it has already been deduced [9] that functionally key residues in anginex are primarily hydrophobic residues, i.e. Leu^5, Val^7, Ile^{20}, Val^{22} and Leu^{24}. Because of this, cysteine residues replaced residues primarily at positions that would be on the hydrophilic face of the amphipathic anginex β-sheet. Moreover, to simplify peptide synthesis and purification, six functionally non-essential residues at the C-terminus of anginex [9] were removed, creating a peptide 27mer analogue of anginex that is shown in the present study to be equipotent with the parent peptide. Double-substituted cysteine pairs were made: Cys^6–Cys^{25}, Cys^8–Cys^{23}, Cys^{10}–Cys^{21}, Cys^{12}–Cys^{19}, Cys^{13}–Cys^{18}, Cys^{13}–Cys^{19} and Cys^6–Cys^{26}. These disulphide-bridged analogues were analysed in three functional assays: EC proliferation, apoptosis and *in vitro*

Abbreviations used: BPI protein, bactericidal-permeability increasing protein; bFGF, basic fibroblast growth factor; CP, cyclicized peptide; EC, endothelial cell; HUVEC, human umbilical-vein EC; NOE, nuclear Overhauser effect; PF4, platelet factor-4; PFG, pulsed-field gradient; PI, propidium iodide; RMS, root mean square.

[1] To whom correspondence should be addressed (e-mail mayox001@umn.edu).

angiogenesis. Peptide conformation was assessed with CD and ^{1}H NMR spectroscopies.

EXPERIMENTAL

Peptide preparation

Peptides were synthesized using fluoren-9-ylmethoxycarbonyl ('Fmoc') chemistry on a Milligen/Biosearch 9600 peptide solid-phase synthesizer, as described previously [8,9]. To form intramolecular disulphide bonds, crude peptides were solubilized at low concentrations (100 μM) and cysteine residues were oxidized by slowly bubbling wet oxygen gas into a stirred aqueous solution overnight at room temperature. Freeze-dried crude peptides (oxidized) were purified by preparative reverse-phase HPLC on a C18 column with an elution gradient of 0–60 % (v/v) acetonitrile with 0.1 % (v/v) trifluoroacetic acid in water. Purity and composition of the peptides were verified by HPLC (Beckman Model 6300), amino acid analysis and MS. The presence of the disulphide bond was checked in all peptides by using 5,5′-dithiobis-(2-nitrobenzoic acid (Ellman's reagent; 'DTNB') pre- and post-treatment with dithiothreitol.

CD

Aqueous solutions for CD were prepared by dissolving the freeze-dried peptide in the appropriate amount of water to give final peptide concentrations of 0.1 mM at pH 5.5. Concentrations were verified by tryptophan absorption at 280 nm. CD spectra were recorded on a Jasco J-710 spectrophotometer using either a 0.01 cm or 0.1 cm path-length thermally jacketed quartz cuvette maintained at 24 or 37 °C with a NesLab water bath. Acquisition was performed using a 50 nm/min scan rate, 1 nm bandwidth and 2 s response. The appropriate baseline was subtracted from each spectrum. Reported spectra are averages of six scans and are expressed as mean residue ellipticity. CD basis spectra (α-helix, β-sheet and random coil) were measured with poly(lysine) and poly(glutamic acid) (Sigma) using conditions and parameters reported previously [16,17]. Experimental CD spectra were fitted with a linear combination of α-helix, β-sheet and random coil basis spectra to estimate secondary structure contributions.

NMR measurements

For NMR measurements, the freeze-dried peptide was dissolved in water at a concentration of approx. 2 mM. The pH was adjusted to pH 5.5 by adding microlitre quantities of NaOH or HCl to the peptide sample. NMR spectra were acquired on a Varian UNITY Plus-600 NMR spectrometer using a homonuclear approach described previously [8]. Data were processed directly on the spectrometer or offline using VNMR (Varian, Inc., Palo Alto, CA, U.S.A.) or NMRPipe [18] on an SGI workstation and were analysed using Sparky (T. D. Goddard and D. G. Kneller, SPARKY 3, University of California, San Francisco, CA, U.S.A.).

Since cyclicized peptides (CPs) are relatively hydrophobic and amphipathic, pulsed-field gradient (PFG)-NMR self-diffusion measurements were performed as a check for peptide aggregation. PFG-NMR experiments were performed and analysed as described by Mayo et al. [10] using a Varian Unity-Plus 500 NMR spectrometer. The maximum magnitude of the gradient was 60 G/cm, and the PFG longitudinal eddy-current delay pulse sequence was used for all self-diffusion measurements which were performed in ^2H_2O at temperatures of 5 °C and 40 °C. Peptide concentrations ranged from 0.1–2 mM.

Structural modelling

Analysis of nuclear Overhauser effect (NOE) data and structural modelling (using X-PLOR [19]) were performed essentially as described previously [20]. Calculated structures were superimposed using the SwissPdbViewer [21] or Insight II (Accelrys, Inc., San Diego, CA, U.S.A.) and were analysed using X-PLOR analysis routines.

Human umbilical-vein EC (HUVEC) cultures

HUVECs were harvested from normal human umbilical cords by perfusion with 0.125 % (w/v) trypsin/EDTA. Harvested HUVECs were cultured in gelatin-coated tissue-culture flasks and subcultured 1:3 once a week in culture medium [RPMI-1640 with 20 % (v/v) human serum supplemented with 2 mM glutamine, 100 units/ml penicillin and 0.1 mg/ml streptomycin].

Proliferation measurement

EC proliferation was measured using a [^{3}H]thymidine incorporation assay. HUVECs were seeded at 5000 cells/well in flat-bottomed tissue-culture plates and grown for 3 days in culture medium in the absence or presence of regulators. During the last 6 h of the assay, the culture was pulsed with 0.5 μCi of [*methyl*-^{3}H]thymidine/well. Results are expressed as the arithmetic mean c.p.m. of triplicate cultures.

Apoptosis measurement

HUVECs were cultured in fibronectin-coated tissue-culture flasks in culture medium [22]. Apoptosis was measured by determination of subdiploid cells after DNA extraction and subsequent staining with propidium iodide (PI) as described previously [23]. Briefly, HUVECs were cultured for 3 days in the presence of 10 ng/ml basic fibroblast growth factor (bFGF) and the conditions as mentioned above. Serum deprivation of HUVECs was used as a positive control for apoptosis. Cells were then harvested and subsequently fixed and permeabilized in 70 % (v/v) ethanol at − 20 °C. After at least 2 h, the cells were centrifuged and resuspended in DNA extraction buffer [45 mM Na_2HPO_4, 2.5 mM citric acid and 0.1 % Triton X-100 (pH 7.4)] for 20 min. PI was added to a final concentration of 20 mg/ml and red log-scale fluorescence was analysed on a FACS-calibur. Apoptosis was quantified as the percentage of cells with PI fluorescence below the fluorescence of cells in the G_0/G_1 (diploid) phase of the cell cycle. Cells with PI fluorescence less than 10 % of cells in G_0/G_1 phase were regarded as cells in the advanced stages of cell death.

In vitro angiogenesis assay

Sprouting and tube formation of bovine ECs were studied using Cytodex-3 beads overgrown with bovine ECs in a three-dimensional collagen gel (vitrogen-100; Collagen Corp., Fremont, CA, U.S.A.) as described by van der Schaft et al. [24]. Following gelation, culture medium containing 20 ng/ml bFGF, with or without anginex or CP analogues, was applied on top of the gel. Photographs were taken after 24 h of cell culture at 37 °C. Sprouts were traced on transparent paper and digitized by scanning using HPscan software. Analysis of the amount of sprouting was performed by binarization of the file and

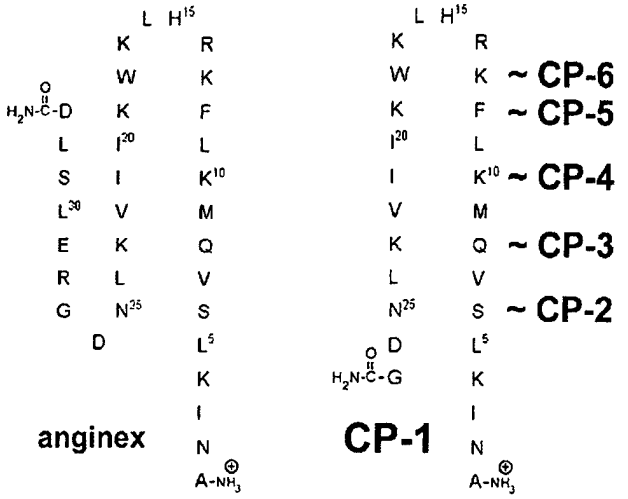

Figure 1 Amino acid sequence and structure of anginex and CP analogues

The amino acid sequence of anginex is shown conformed as an anti-parallel β-sheet on the left-hand side of the Figure. The N-terminus is at the right bottom as labelled. CP analogues have only the first 27 residues and therefore are devoid of C-terminal residues Arg-Glu-Lys-Ser-Lys-Asp. The new C-terminal residue has its backbone carboxylate group amidated. The amino acid sequence for the control linear peptide 27mer (no cysteine residues) CP-1 is given on the right-hand side of the Figure. CP-2 to CP-6 [i.e. CP-2 (Cys^6–Cys^{25}), CP-3 (Cys^8–Cys^{23}), CP-4 (Cys^{10}–Cys^{21}), CP-5 (Cys^{12}–Cys^{19}), CP-6 (Cys^{13}–Cys^{18})] have the same sequence as CP-1, with disulphide bridges positioned between β-strand 1 and β-strand 2 as indicated. CP-7 [Cys^{13}–Cys^{19}] and CP-8 [Cys^6–Cys^{26}] are control peptides that alter the alignment of β-strands 1 and 2. Single-letter amino-acid notation is used.

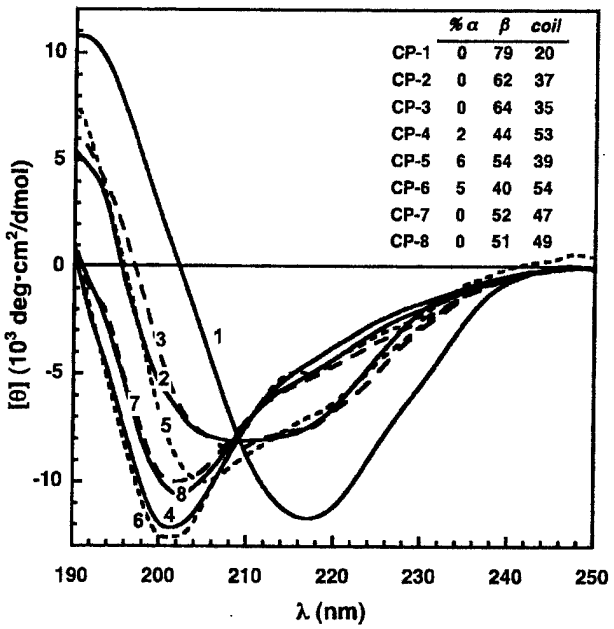

Figure 2 CD spectra for CP analogues

Far-UV CD spectra for CP analogues are shown as mean residue ellipticity ([θ]) versus wavelength. All spectra display a mixture of β-sheet and random coil conformations, as shown by linear fits of basis spectra (inset). Spectra shown were obtained at 37 °C; spectra at 24 °C were comparable. Peptide concentration was 0.1 mM in H_2O, pH 5.5. Other experimental conditions are given in the Experimental section.

quantification of sprout pixel count using Scion Image software, which yields a measure of sprout length [25].

RESULTS AND DISCUSSION

For the CP series, all CP analogues have the same sequence as anginex minus the six C-terminal residues Arg-Glu-Leu-Ser-Leu-Asp (Figure 1). CP-1 is the control linear peptide 27mer (no cysteine residues), and CP-2 to CP-8 are double-cysteine-substituted disulphide-bridged peptides: Cys^6–Cys^{25} (CP-2), Cys^8–Cys^{23} (CP-3), Cys^{10}–Cys^{21} (CP-4), Cys^{12}–Cys^{19} (CP-5), Cys^{13}–Cys^{18} (CP-6), Cys^{13}–Cys^{19} (CP-7) and Cys^6–Cys^{26} (CP-8). The amino acid sequences for parent anginex and CP-1 are given in Figure 1, and positions for disulphide bonds in CP-2 to CP-6 are indicated by curved lines at the right of the CP-1 sequence. Because functionally key residues in anginex are primarily hydrophobic, i.e. Leu^5, Val^7, Ile^{20}, Val^{22} and Leu^{24}, and would lie on one side of the amphipathic structure in a β-sheet conformation [9], residues on the hydrophilic face (and not the hydrophobic face) of the proposed β-sheet were substituted with cysteine residues. For assurance that cysteine-substituted positions did not affect activity of the parent peptide, single-substituted alanine variants ($Ser^6 \rightarrow Ala$, $Gln^8 \rightarrow Ala$, $Lys^{10} \rightarrow Ala$, $Phe^{12} \rightarrow Ala$, $Lys^{13} \rightarrow Ala$, $Trp^{18} \rightarrow Ala$, $Lys^{19} \rightarrow Ala$, $Ile^{21} \rightarrow Ala$, $Lys^{23} \rightarrow Ala$, $Asn^{25} \rightarrow Ala$ and $Asp^{26} \rightarrow Ala$) were also made and tested in the *in vitro* EC proliferation assay. Relative to the parent peptide, activities were unaffected solely by amino acid substitutions at these positions (results not shown). On forming an actual β-sheet in CP-2 to CP-6, positioning of disulphide bonds constrains the β-strand alignment to be the same as that proposed for the folding of anginex [8]. CP-7 [$Lys^{13} \rightarrow Cys$ and $Lys^{19} \rightarrow Cys$] and CP-8 [$Ser^6 \rightarrow Cys$ and $Asp^{26} \rightarrow Cys$] are control peptides that shift the β-strand alignment by one residue to be out of register with the other CP analogues.

CD

CD and NMR spectroscopies were used to assess the conformation of CP analogues. For all CP analogues, far-UV CD traces indicated a mixture of β-sheet and random coil conformations (Figure 2), with the degree of β-sheet character corresponding to the intensity of the characteristic 217 nm trough [17,26,27]. Linear combinations of secondary structure basis spectra (α-helix, β-sheet and random coil) fitted to the CP analogue spectra (Figure 2, inset) showed the largest β-sheet content (79%) in the linear CP-1 peptide and the smallest (40%) in CP-6. Fitted data indicate the absence of helical content for most of the CP analogues. Even though CP-4, CP-5 and CP-6 show 2–6% helix content, this contribution is small enough that it is within the error from the fitting process. In addition, because the CP analogues are relatively flexible, the secondary structure contributions are only meant to semi-quantify the trend in β-sheet content. Nevertheless, the CP analogue conformational distributions are consistent with that for anginex [11].

^{1}H NMR conformational analysis

Even though CD data demonstrate the presence of significant populations of β-sheets in all CP analogues, proton NMR spectra for all CP analogues, except CP-2, are characteristic of mostly random coil conformations (results not shown). CP-2 is the only CP analogue that shows well-dispersed resonances indicative of a well-folded structure [28,29]. Since the parent anginex peptide exists in solution in a monomer/dimer/tetramer equilibrium [29,30], PFG-NMR self-diffusion measurements were performed on CP analogues (results not shown). Analysis of the CP analogue diffusivities indicates that, at a concentration of 2 mM, CP-2 is mostly dimeric, whereas the other CP analogues are a mixture

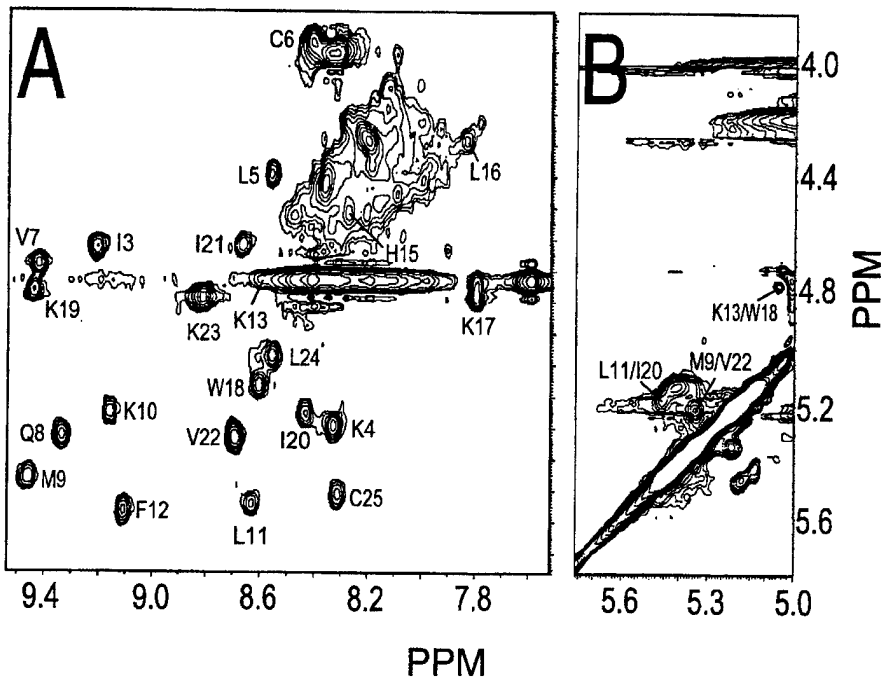

Figure 3 TOCSY and NOESY spectra for CP-2

600 MHz ^{1}H TOCSY (**A**) and NOESY (**B**) spectra are shown for CP-2. Peptide concentration was 2.3 mM in $H_2O/^2H_2O$ (9:1, v/v), pH 5.5 at 40 °C. Spectra were accumulated with 8000 data points over 8000 Hz sweep width and were processed with 1 Hz line broadening. Only spectral regions downfield from the partially deuterated water resonance are shown and some key NOEs are identified. Several cross-peaks have been labelled to indicate intra- and inter-monomer αH–αH NOEs, which have been used to indicate β-strand alignment. In (**B**), the cross-peaks are labelled with two numbers separated by a solidus to indicate which residues in the sequence are involved. Single-letter amino-acid notation has been used.

of dimers and monomers. None of the CP analogues apparently associates with the tetramer state like anginex.

NMR structure of CP-2

Because initial NMR experiments indicated that CP-2 is well-folded, a complete NMR structure analysis of this peptide was performed. The αH-NH region of a TOCSY plot of CP-2 shows high frequency dispersion of NH and αH resonances, indicating the presence of a well-folded β-sheet conformation (Figure 3A). This is also evident by the observation of cross-strand αH-αH NOEs (Figure 3B and Figure 4A). Structurally, these NOESY data indicate the presence of the same anti-parallel β-sheet strand alignment as observed in βpep-4 and other βpep peptides [11].

For CP-2, conformational modelling was performed using NOE data acquired for the peptide. A total of 160 NOE distance constraints were derived from analysis of NOESY spectra. These include 94 intra-residue, 22 sequential, 16 medium-range ($|i-j|<5$) and 28 long-range ($|i-j|>5$) constraints. In addition, a total of eight hydrogen bonds were identified by inspection of initial CP-2 structures and from long-lived backbone NHs, giving rise to 16 hydrogen bond distance constraints. The total number of experimentally derived constraints was therefore 168, giving an average of six constraints/residue. Initially, 100 structures for CP-2 were calculated as described in the Experimental section. The best-fit superpositions of backbone Cα atoms for the final 18 structures are shown in Figure 4(B). These structures showed no NOE violations greater than 0.5 Å (where 1 Å = 0.1 nm). Structural statistics (Table 1) show that the N-terminus is somewhat less structurally defined and that the structures satisfy experimental constraints quite well. In addition, Φ and ψ angular order parameters are all >0.8. Taken together, the above data indicate that the structures used to represent the solution conformation of CP-2 are well converged. The root mean square (RMS) deviation for backbone atoms of β-sheet residues

Table 1 Structural statistics for the calculated structures of CP-2 from NMR data

RMS deviations values are means ± S.D. for the 18 structures. Energy values represent means ± S.D.

Parameters	
RMS deviations from experimental distance restraints (Å)*	
NOE ($n=176$)	0.047 ± 0.007
H-bond ($n=16$)	
RMS deviations from idealized geometry	
Bonds (Å)	0.003
Angles (°)	0.5 ± 0.02
Impropers (°)	0.37 ± 0.02
Energies (kJ · mol^{-1})	
E_{NOE}†	21.3 ± 2.5
E_{BOND}	15.98 ± 2.5
E_{ANGLE}	164.8 ± 11.7
$E_{IMPROPER}$	80.3 ± 23.8
E_{TOTAL}	335.6 ± 43.1

*None of the 18 final structures exhibited distance restraint violations greater than 0.5 Å or dihedral angle violations greater than 5°.

†The final value of the NOE (E_{NOE}) was calculated with a force constant of 210 kJ · mol^{-1} · Å^{-2}.

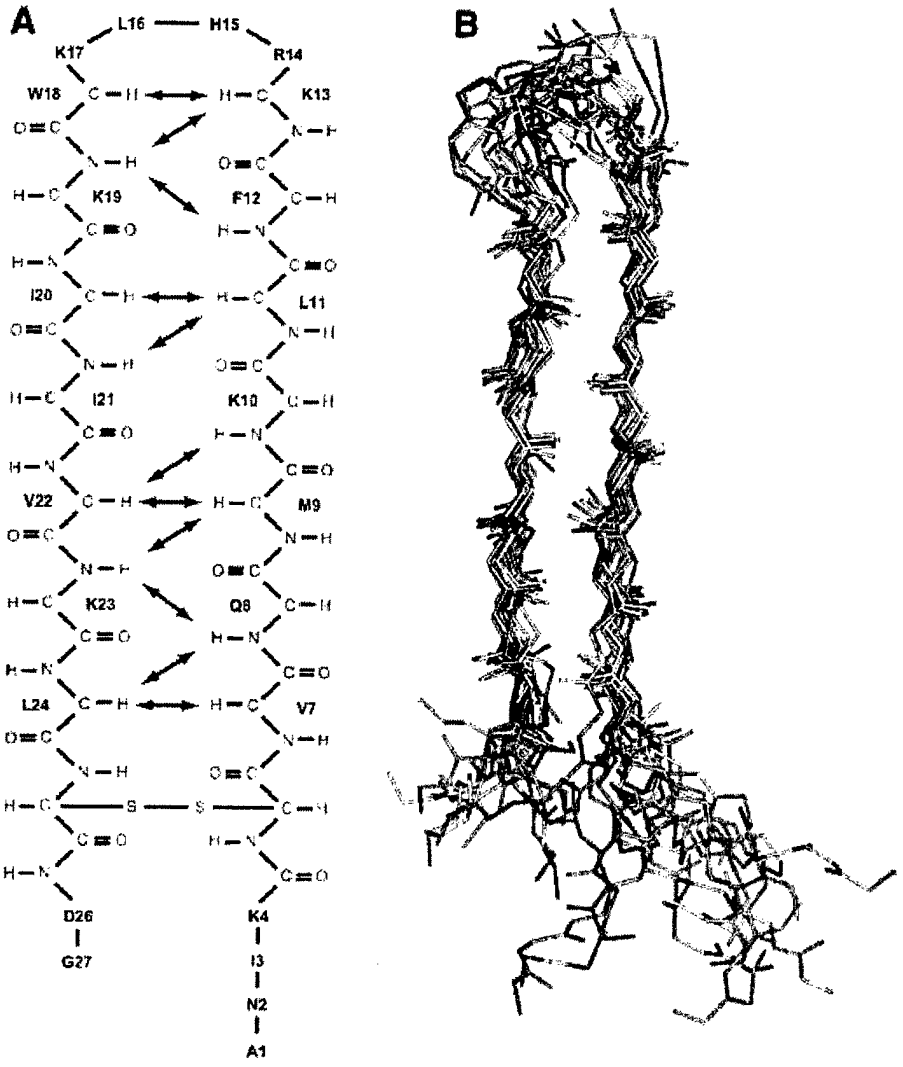

Figure 4 NOE-derived structures of CP-2

(**A**) Key cross-strand NOEs and the overall fold for CP-2. Single-letter amino-acid notation is used. The best-fit superpositions of backbone Cα atoms for the final 18 structures are shown in (**B**). The RMS deviation for backbone atoms of β-sheet residues 6–12 and 19–25 (excluding terminal and loop residues) is 0.61 Å, and for backbone atoms of residues 6–25 (excluding N- and C-terminal residues) it is 1.13 Å.

6–12 and 19–25 (excluding terminal and loop residues) is 0.61 Å and for backbone atoms of residues 6–25 (excluding N- and C-terminal residues) is 1.13 Å.

Even though only CP-2 is well-folded as an anti-parallel β-sheet, it is most probable that peptides CP-3, CP-4, CP-5 and CP-6 share the same overall β-sheet fold, because they only differ in the position of the disulphide bridge.

CP analogues inhibit EC proliferation

CP analogues were tested for their ability to inhibit the proliferation of growth-factor-induced (bFGF, 10 ng/ml) HUVECs in the [^{3}H]thymidine incorporation assay [15]. Relative to the activity of the parent peptide anginex [8], CP analogues effectively inhibited the proliferation of HUVECs to various extents (Figure 5). Although the linear control, CP-1, and three of the disulphide-bridged variants, CP-4, CP-5 and CP-6, were essentially as effective as anginex, CP-2 and CP-3 appeared to be almost as active, and control peptides CP-7 and CP-8 were only slightly active. The kinetics of these anti-proliferative effects on ECs were similar to those found for anginex, with half-maximal effects after 36–40 h and maximal responses after 3 days. As with anginex, the inhibition of proliferation by CP analogues was specific for ECs, since proliferation of fibroblasts obtained from human endometrium was unaffected (results not shown).

CP analogues promote apoptosis in ECs

To investigate whether CP-induced inhibition of EC growth is based on specific induction of apoptosis in these cells, as was demonstrated for anginex [8], HUVECs were exposed to 25 μM peptide for 48 h, and the percentage of cells undergoing apoptosis was quantified by analysis of DNA fragmentation following DNA extraction, PI staining and flow cytometric analysis. Although all CP analogues demonstrated apoptotic activity, CP-4 and CP-5 were the most active and even slightly more effective, on average,

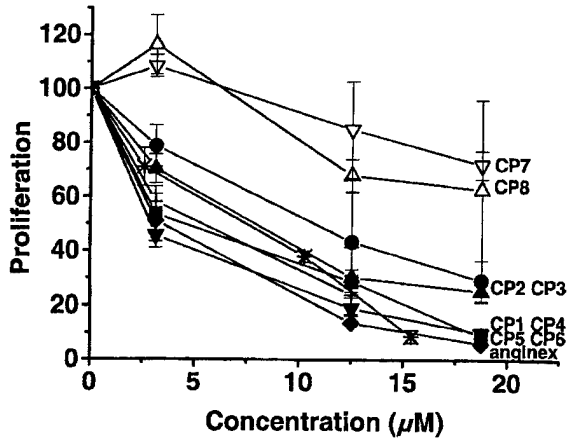

Figure 5 Inhibition of EC proliferation by CP analogues

Proliferation of bFGF-stimulated (10 ng/ml) HUVEC cultures was measured by quantification of [^{3}H]thymidine incorporation. Proliferation is expressed as mean c.p.m. ($\pm$S.E.M.) of quadruplicate cultures of four independent experiments. Dose–response curves of CP analogues and parent anginex on bFGF-stimulated HUVEC proliferation are shown.

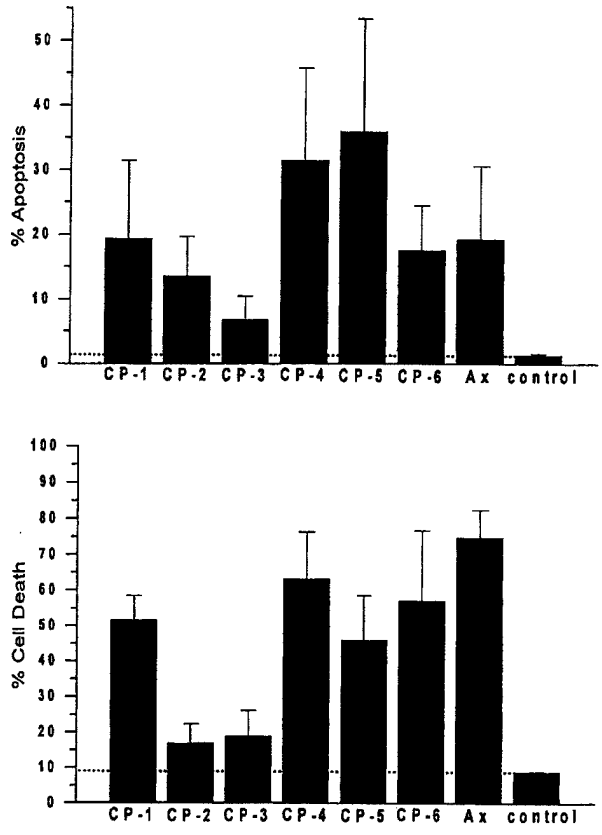

Figure 6 CP analogues induce apoptosis in ECS

HUVECs were cultured for 2 days in the absence or presence of 25 μM CP analogues or anginex (Ax). Upper panel, apoptosis induction was demonstrated by analysis of subdiploid cells after DNA extraction and staining with PI. Lower panel, total number of dead cells was determined by total number of diploid cells as quantified by FACS analysis. Quantification of the means ($\pm$S.E.M.) of four different experiments is shown.

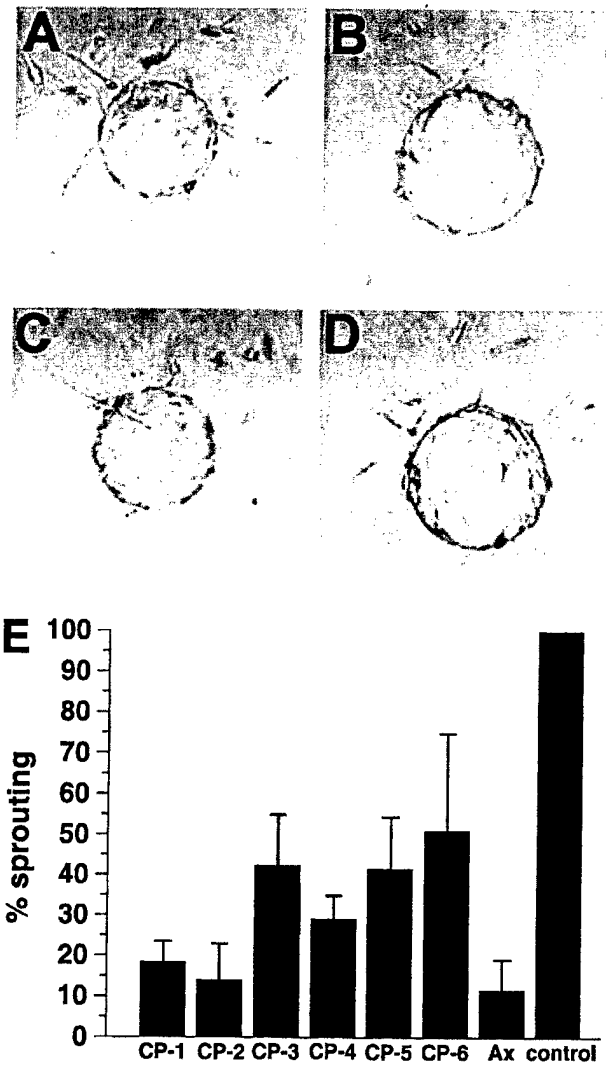

Figure 7 Anginex inhibits *in vitro* angiogenesis in a collagen matrix

Bovine ECs were cultured on gelatin-coated Cytodex-3 beads in a collagen matrix. Sprouting was induced by addition of 20 ng/ml bFGF and 25 μM of the CP analogues or anginex (Ax) was added when tested. Tube formation of a representative experiment under control conditions (**A**; pixel count 1002) and in the presence of anginex (**B**; pixel count 211), CP-1 (**C**; pixel count 205) and CP-6 (**D**; pixel count 513) is shown. CP-7 had a pixel count of 990. Mean size of the beads is 170 $\pm$ 40 μm. (**E**) Quantification of the means ($\pm$S.E.M.) of four different experiments.

than anginex (Figure 6A). Since apoptosis in this assay is defined as those subdiploid cells with a minimum of 10% of the DNA content of the diploid cells, advanced or late stage apoptosis may result in less than 10% of that value. Consequently, the total number of dead cells was also quantified (Figure 6B). The loss of ECs in G_2 and M ($4n$ DNA) phases of the cell cycle is approx. 10% or less (results not shown). The correlation between apoptosis induction and anti-proliferative effects suggests that CP analogues, like anginex, regulate EC growth by forcing ECs to undergo apoptosis.

In vitro angiogenesis assay

Since angiogenesis is a complex process, which, aside from EC proliferation, depends on cell migration and differentiation, the

effects of CP analogues on angiogenesis were investigated in an *in vitro* collagen matrix-based sprout formation assay [13–15]. Figures 7(A–D) show raw data from this angiogenesis assay, and Figure 7(E) gives the percentage of sprouting relative to control, as detailed in the Figure legend and the Experimental section. Although all CP analogues were able to inhibit sprout formation to various extents, the best responses, comparable with those from anginex, were observed with CP-1 and CP-2. It was somewhat surprising that CP-4, CP-5 and CP-6, which were the most effective at inhibiting EC proliferation, were not as effective in this assay. One reason for this could be the complexity of the collagen gel sprouting assay itself. Because these peptides must first navigate through the gel before exerting their effect on ECs, it may be that CP-1 and CP-2 permeate the gel better than other CP analogues or interact somewhat differently with the gel matrix. Alternatively, it may be that the sprouting assay is indeed the more sensitive indicator of anti-angiogenic potential. In any event, bioactivity in this angiogenesis assay decreased most when the β-strand alignment was shifted, as in CP-7 and CP-8, indicating that that specific strand alignment is crucial to maintaining full bioactivity.

Conclusions

In the present study, we demonstrate that the bioactive conformation of the anti-angiogenic anginex peptide is an anti-parallel β-sheet. This finding is consistent with earlier results [8,9] on anginex that in the β-sheet conformation all five hydrophobic residues (Leu^5, Va^{17}, Ile^{20}, Val^{22} and Leu^{24}), which were identified as being crucial to anti-proliferative activity, are proximal and are conformed on the hydrophobic face of the amphipathic β-sheet [9]. Comparison of the three-dimensional structures of several anti-angiogenic proteins, e.g. endostatin [31], PF4 [32], tumour necrosis factor [33] and BPI protein [34], provides a higher level of structural commonality among anti-angiogenic proteins in that they are comprised primarily of anti-parallel β-sheet structure. Furthermore, a survey of amino acid sequences from numerous anti-angiogenic proteins reveals that they are compositionally similar, containing numerous hydrophobic and cationic residues. These structural and compositional characteristics, which appear to be functionally important, are embodied in anginex [9]. As structure–function relationships in these and other anti-angiogenic proteins and peptides become known, it will be interesting to see if this is a common feature among anti-angiogenic proteins. Knowing that this β-sheet conformation is that which promotes anti-angiogenic activity will aid in the development of small molecule mimetics of the anginex peptide.

This work was supported by generous support from the National Institutes of Health (NIH CA-96090), the US Department of Defense (Army Grant # DA/DAMD17-99-1-9564), the Dutch Cancer Society, and ActiPep Biotechnology, Inc. N. A. L. was supported by a Whitaker Foundation Graduate Fellowship. NMR instrumentation was provided with funds from the NSF (BIR-961477) and the University of Minnesota Medical School. We are also grateful to Dinesha Walek of the University of Minnesota Microchemical Facility for peptide synthesis.

REFERENCES

1 Folkman, J. (1995) Angiogenesis in cancer, vascular, rheumatoid and other disease. Nat. Med. **1**, 27–31
2 Griffioen, A. W. and Molema, G. (2000) Angiogenesis: potentials for pharmacologic intervention in the treatment of cancer, cardiovascular diseases, and chronic inflammation. Pharmacol. Rev. **52**, 237–268
3 Gupta, S. K. and Singh, J. P. (1994) Inhibition of endothelial cell proliferation by platelet factor-4 involves a unique action on S phase progression. J. Cell Biol. **127**, 1121–1127
4 Rastinejad, F., Polverini, P. J. and Bouck, N. P. (1989) Regulation of the activity of a new inhibitor of angiogenesis by a cancer suppressor gene. Cell (Cambridge, Mass.) **56**, 345–355
5 O'Reilly, M. S., Holmgren, L., Shing, Y., Chen, C., Rosenthal, R. A., Moses, M., Lane, W. S., Cao, Y., Sage, E. H. and Folkman, J. (1994) Angiostatin: a novel angiogenesis inhibitor that mediates the suppression of metastases by a Lewis lung carcinoma. Cell (Cambridge, Mass.) **79**, 315–328
6 O'Reilly, M. S., Boehm, T., Shing, Y., Fukai, N., Vasios, G., Lane, W. S., Flynn, E., Birkhead, J. R., Olsen, B. R. and Folkman, J. (1997) Endostatin: an endogenous inhibitor of angiogenesis and tumor growth. Cell (Cambridge, Mass.) **88**, 277–285
7 van der Schaft, D. W., Toebes, E. A., Haseman, J. R., Mayo, K. H. and Griffioen, A. W. (2000) Bactericidal/permeability-increasing protein (BPI) inhibits angiogenesis via induction of apoptosis in vascular endothelial cells. Blood **96**, 176–181
8 Griffioen, A. W., van der Schaft, D. W., Barendsz-Janson, A. F., Cox, A., Struijker Boudier, H. A., Hillen, H. F. and Mayo, K. H. (2001) Anginex, a designed peptide that inhibits angiogenesis. Biochem. J. **354**, 233–242
9 Mayo, K. H., van der Schaft, D. W. and Griffioen, A. W. (2001) Designed β-sheet peptides that inhibit proliferation and induce apoptosis in endothelial cells. Angiogenesis **4**, 45–51
10 Mayo, K. H., Ilyina, E. and Park, H. (1996) A recipe for designing water-soluble, β-sheet-forming peptides. Protein Sci. **5**, 13001–11315
11 Ilyina, E., Roongta, V. and Mayo, K. H. (1997) NMR structure of a *de novo* designed, peptide 33mer with two distinct, compact β-sheet folds. Biochemistry **36**, 5245–5250
12 Mayo, K. H., Haseman, J. R., Ilyina, E. and Gray, B. (1998) Designed β-sheet-forming peptide 33mers with potent human bactericidal/permeability increasing protein-like bactericidal and endotoxin neutralizing activities. Biochim. Biophys. Acta **1425**, 81–92
13 van der Schaft, D. W., Dings, R. P., de Lussanet, Q. G., van Eijk, L. I., Nap, A. W., Beets-Tan, R. G., Bouma-Ter Steege, J. C., Wagstaff, J., Mayo, K. H. and Griffioen, A. W. (2002) The designer anti-angiogenic peptide anginex targets tumor endothelial cells and inhibits tumor growth in animal models. FASEB J. **16**, 1991–1993
14 Dings, R. P., Yokoyama, Y., Ramakrishnan, S., Griffioen, A. W. and Mayo, K. H. (2003) The designed angiostatic peptide anginex synergistically improves chemotherapy and antiangiogenesis therapy with angiostatin. Cancer Res. **63**, 382–385
15 Dings, R. P. M., van der Schaft, D. W., Hargittai, B., Haseman, J. R., Griffioen, A. W. and Mayo, K. H. (2003) Anti-tumor activity of the novel angiogenesis inhibitor anginex. Cancer Lett. (Shannon, Irel.) **194**, 55–66
16 Adler, A. J., Greenfield, N. J. and Fasman, G. D. (1973) Circular dichroism and optical rotary dispersion of proteins and polypeptides. Methods Enzymol. **27**, 675–735
17 Greenfield, N. and Fasman, G. D. (1969) Computed circular dichroism spectra for the evaluation of protein conformation. Biochemistry. **8**, 4108–4116
18 Delaglio, F., Grzesiek, S., Vuister, G. W., Zhu, G., Pfeifer, J. and Bax, A. (1995) NMRPipe: a multidimensional spectral processing system based on UNIX pipes. J. Biomol. NMR. **6**, 277–293
19 Brunger, A. T. (1992) X-plor Manual, Yale University Press, New Haven
20 Mayo, K. H., Haseman, J., Young, H. C. and Mayo, J. W. (2000) Structure–function relationships in novel peptide dodecamers with broad-spectrum bactericidal and endotoxin-neutralizing activities. Biochem. J. **349**, 717–728
21 Guex, N. and Peitsch, M. C. (1997) SWISS-MODEL and the Swiss-PdbViewer: an environment for comparative protein modeling. Electrophoresis **18**, 2714–2723
22 Relou, I. A., Damen, C. A., van der Schaft, D. W., Groenewegen, G. and Griffioen, A. W. (1998) Effect of culture conditions on endothelial cell growth and responsiveness. Tissue Cell **30**, 525–530
23 Darzynkiewicz, Z., Bruno, S., Del Bino, G., Gorczyca, W., Hotz, M. A., Lassota, P. and Traganos, F. (1992) Features of apoptotic cells measured by flow cytometry. Cytometry **13**, 795–808
24 van der Schaft, D. W., Wagstaff, J., Mayo, K. H. and Griffioen, A. W. (2002) The antiangiogenic properties of bactericidal/permeability-increasing protein (BPI). Ann. Med. **34**, 19–27
25 Wild, R., Ramakrishnan, S., Sedgewick, J. and Griffioen, A. W. (2000) Quantitative assessment of angiogenesis and tumor vessel architecture by computer-assisted digital image analysis: effects of VEGF-toxin conjugate on tumor microvessel density. Microvasc. Res. **59**, 368–376
26 Johnson, W. C. J. (1990) Protein secondary structure and circular dichroism: a practical guide. Proteins **7**, 205–214
27 Waterhous, D. V. and Johnson, Jr, W. C. (1994) Importance of environment in determining secondary structure in proteins. Biochemistry **33**, 2121–2128
28 Hanzawa, H., Shimada, I., Kuzuhara, T., Komano, H., Kohda, D., Inagaki, F., Natori, S. and Arata, Y. (1990) 1H nuclear magnetic resonance study of the solution conformation of an antibacterial protein, sapecin. FEBS Lett. **269**, 413–420
29 Selsted, M. E. and Harwig, S. S. (1989) Determination of the disulfide array in the human defensin HNP-2. A covalently cyclized peptide. J. Biol. Chem. **264**, 4003–4007

30 Bodenhausen, G., Vold, R. L. and Vold, R. R. (1980) Multiple quantum spin echo spectroscopy. J. Magn. Reson. **37**, 93–99
31 Hohenester, E., Sasaki, T., Olsen, B. R. and Timpl, R. (1998) Crystal structure of the angiogenesis inhibitor endostatin at 1.5 Å resolution. EMBO J. **17**, 1656–1664
32 Mayo, K. H., Roongta, V., Ilyina, E., Milius, R., Barker, S., Quinlan, C., La Rosa, G. and Daly, T. J. (1995) NMR solution structure of the 32-kDa platelet factor 4 ELR-motif N-terminal chimera: a symmetric tetramer. Biochemistry **34**, 11399–11409
33 Baeyens, K. J., De Bondt, H. L., Raeymaekers, A., Fiers, W. and De Ranter, C. J. (1999) The structure of mouse tumour-necrosis factor at 1.4 Å resolution: towards modulation of its selectivity and trimerization. Acta Crystallogr., Sect.D: Biol. Crystallogr. **55**, 772–778
34 Beamer, L. J., Carroll, S. F. and Eisenberg, D. (1997) Crystal structure of human BPI and two bound phospholipids at 2.4 Å resolution. Science (Washington, D.C.) **276**, 1861–1864

Received 21 February 2003/22 April 2003; accepted 23 April 2003
Published as BJ Immediate Publication 23 April 2003, DOI 10.1042/BJ20030295

Angiogenesis 6: 000–000, 2003.

Review

Discovery and development of anti-angiogenic peptides: A structural link

Ruud P.M. Dings[1,2], Irina Nesmelova[1], Arjan W. Griffioen[2] & Kevin H. Mayo[1]
[1]*Department of Biochemistry, Molecular Biology and Biophysics, University of Minnesota Health Sciences Center, 321 Church Street, Minneapolis, Minnesota 55455, USA;* [2]*Angiogenesis Laboratory, Research Institute for Growth and Development (GROW), Depts of Internal Medicine and Pathology, University Hospital and Maastricht University, P.O. Box 5800, 6202 AZ Maastricht, The Netherlands*

Received 20 January 2003; accepted in revised form 1 May 2003

Key words: angiogenesis inhibition, angiostatic peptides, angiostatic proteins, designer peptides and review

Abstract

Cancer is a disease promoted by excess angiogenesis. Interference with this process poses an attractive approach to controling aberrant tumor growth, a hypothesis first proposed in the early 1970s that led to world-wide focus on identifying and developing angiogenesis inhibitors, which currently number in the hundreds. This review surveys the discovery and development of anti-angiogenic protein fragments and peptides, with a slant towards understanding their structure–function relationships to aid in the design of better therapeutic agents.

Introduction

Although it was hypothesized some 30 years ago that inhibition of angiogenesis could attenuate tumor growth [1, 2], it was only after the isolation, identification and *in vivo* testing of the angiogenic inhibitory protein fragments angiostatin [3] and endostatin [4] that Folkman's hypothesis gained general acceptance. Since that time, numerous angiogenesis inhibitors (over 300) have been identified, a number of which are currently in various phases of human cancer trials (http://cancertrials.nci.nih.gov). Even though a few anti-angiogenic compounds have demonstrated promise in the clinic, no major clinical breakthroughs have been reported using a stand-alone anti-angiogenic agent as a therapeutic, and even some of these compounds have failed in clinical testing (e.g. SU5416, BB2516, AG3340, Bay 12-9566, IM-862 [5]). This underscores the need to identify and develop more and better angiogenesis inhibitors and to perform clinical studies with them either as monotherapy or in combination with conventional treatment strategies.

Tumor angiogenesis is a highly complex biological process, and blocking only one step of this process may merely force a growing tumor to circumvent the particular blocked pathway. Tumors have in their arsenal a number of ways to promote angiogenesis, and anti-angiogenics can inhibit neovascularization at different steps in the formation of new blood vessels. For example, agents that block specific angiogenic ligands, e.g. VEGF, or their receptor-mediated signaling pathway(s) only block one of the angiogenic factors secreted by tumors, leaving open the possibility that a tumor can adapt and switch angiogenic stimulators, e.g. from VEGF to FGF, in a second wave of VEGF-independent angiogenesis [6].

The complexity of tumor-induced angiogenesis also rests in the micro-environment of a given tumor, which further complicates development of a highly effective anti-angiogenic agent. For example, hypoxia and ischemia trigger the production of angiogenic survival factors, such as VEGF, but also of endothelial apoptosis-inducing factors like TNF-α [7, 8]. The level of production of these factors is important because some cytokines, such as TNFα and TNFβ, can function both as stimulators and inhibitors of angiogenesis depending upon their concentration. Another example is thrombospondin-2 (TSP-2), which displays anti-angiogenic activity [9, 10], *via* secretion from fibroblasts, and possibly other mesenchymal cells, as a paracrine mediator of EC proliferation [11]. Such agents are therefore contextual inhibitors of angiogenesis that depend on their presence within a particular physiological environment.

Angiogenesis inhibitors have been identified using a myriad of approaches, including (1) isolation and identification of endogenous inhibitors of tumor-promoted angiogenesis [4], (2) gene therapies [12], (3) antibody therapies against pro-angiogenic molecules [13] and (4) their receptors [14], (5) anti-sense approaches

Correspondence to: Kevin H. Maya, Department of Biochemistry, Molecular Biology and Biophysics, University of Minnesota Health Sciences Center, 321 Church Street, Minneapolis, Minnesota 55455, USA. Tel.: +1-612-625-9968; Fax: +1-612-624-5121/625-2163; E-mail: mayox001@tc.umn.edu

[15], (6) soluble growth factor receptors as antagonists [16], (7) interference with growth factor signaling [17], (8) ribozymes [18], (9) small molecule inhibitors [19], and (10) peptide design [20].

Angiogenesis inhibitors, particularly those specific for endothelial cells (ECs), are now also being used as 'homing'-devices for chemotherapeutics in the hope of increasing specificity and reducing toxicity. The tumor-homing capacity of EC-specific peptides was successfully used to target doxorubicin, a frequently used chemotherapeutic with intrinsic anti-angiogenic activity [21]. In xenograft models, this targeting approach resulted in prolonged survival, reduction of the optimal effective dose and reduced toxicity. Targeting can be done either classically by linking the chemotherapeutic chemically to the anti-angiogenic compound or in a novel approach by linking it to peptides which specifically target tumor vasculature [22].

The most promising anti-angiogenics are those that act directly on ECs to inhibit tumor angiogenesis, an approach that is less prone to drug resistance and can be more therapeutically effective against a broad spectrum of tumors. The well-known proteins, angiostatin and endostatin, are two such EC-specific angiogenesis inhibitors. Although there are numerous proteins known to be anti-angiogenic, this review is focused on the discovery and/or development of protein fragments and small peptide inhibitors of angiogenesis. Moreover, this treatise is not meant to be exhaustive; rather it is an attempt to review this literature with a slant towards better understanding structural similarities and structure–function relationships through this general class of anti-angiogenic agents.

Protein fragments

One approach that has been used to identify molecules with anti-angiogenic potential is to isolate components from the serum or body fluids of animals undergoing extensive angiogenesis, i.e., tumor-bearing or pregnant animals. Many, if not most, of these components were found to be fragments of proteins, which, relative to their parent protein that may or may not be anti-angiogenic by themselves, display anti-angiogenic properties when separated from their parent protein. Although endostatin and angiostatin are perhaps the best known examples of such protein fragments, others are discussed below as well.

Angiostatin

The circulating angiogenesis inhibitor angiostatin [3] is a fragment of the non-anti-angiogenic plasma protein plasminogen. Angiostatin contains the first four triple-loop disulfide-linked regions of plasminogen, known as kringle domains [3, 23]. This approximately 40 kDa protein was initially isolated from the serum and urine of mice with Lewis lung carcinoma (LLC). Although elastase cleaves plasminogen into an active form of angiostatin *in vitro*, it is not yet clear which protease(s) is (are) involved in the conversion of plasminogen to angiostatin *in vivo*. However, it was recently suggested that depending on the type of tumor, either tumor cells themselves or tumor-associated macrophages express enzymatic activity capable of converting inactive plasminogen into angiostatin. Although plasminogen itself does not bind to the integrin receptor $\alpha_v\beta_3$, it appears that angiostatin does, suggesting that interaction with $\alpha_v\beta_3$ is, in part, responsible for the anti-angiogenic properties of angiostatin [24]. At least two other possible receptors for angiostatin have been reported: ATP-synthase [25] and integrin $\alpha_9\beta_1$ [24]. Table 1 lists receptors reported for angiostatin and other anti-angiogenic protein fragments and peptides.

Other proteolytic fragments of human plasminogen can also inhibit neovascularization and growth of lung metastases in mice [3]. For example, kringle 1 (K1) potently inhibits EC growth, whereas K4 exhibits almost no anti-angiogenic activity *in vitro* [23]. Interestingly, K5, which is not present in angiostatin, is structurally related to the other four kringles in plasminogen and also exhibits anti-endothelial activity [26].

The crystal structure of three kringles from angiostatin [27] folds, as expected for a kringle-structured protein, into anti-parallel β-sheet and aperiodic loops. These three kringles are organized in an overall L-shape. Because angiostatin contains a nearly equal number of anionic and cationic residues, the surface of the folded protein is relatively neutral. Nonetheless, the most outstanding electrostatic feature of the protein is a highly electropositive lysine-rich binding site. This is a

Table 1. Anti-angiogenic compounds and their reported receptors.

Inhibitor	Receptor	Source
Angiostatin	$\alpha_9\beta_1$	[24]
	$\alpha_v\beta_3$	[24]
	ATP-synthase	[25]
Endostatin	$\alpha_v\beta_3$	[31]
	$\alpha_v\beta_5$	[31]
	Glypicans	[94]
	Tropomyosin	[95]
	$\alpha_5\beta_1$	[30]
PEX	$\alpha_v\beta_3$	[42]
Tumstatin, Tum-5	$\alpha_v\beta_3$	[37]
Anastellin	$\alpha_v\beta_3$	[47]
16K PRL	Yet to be Indentified	
Thrombospondin-1	CD36	[67]
		[96]
	Syndecan	[66]
	HSPG	[66]
	β_1 and β_3 integrins	
	IAP	
	105Kd/80 Kd	[66]
Anginex	EC adhesion /migration receptor	[20]
RGD-containing peptides	$\alpha_v\beta_3$	[48]
	$\alpha_v\beta_5$	[21]
NGR-containing peptides	CD13	

recurring structural/compositional theme for most anti-angiogenic proteins and peptides identified so far: antiparallel β-sheet structure and proponderance of positively charged and hydrophobic residues.

Endostatin

Endostatin was discovered using a similar approach as with angiostatin, albeit with hemangioendothelioma as the tumor source [4]. Like angiostatin, endostatin specifically inhibits proliferation of EC *in vitro* and tumor growth in various mouse models *in vivo*. Furthermore, endostatin has been shown to induce EC apoptosis in the presence of minimal serum. Endostatin is a 20 kDa C-terminal proteolytic fragment of the NC1 domain of collagen XVIII, which is a member of a family of collagen-like proteins referred to as multiplexins and is localized primarily in the extracellular matrix surrounding blood vessels. The multiplexin family of collagens is distinguished by nearly 60% sequence identity within the final 184 residues of their C-terminal globular domains [28], suggesting that any one of these fragments likewise would be anti-angiogenic. This was recently confirmed by the anti-angiogenic activity of restin, the C-terminal non-collagenous region (NC10) of the α1 chain of human type XV collagen [29].

The precise mechanism of action for endostatin remains elusive, primarily because endostatin has been found to interact with multiple 'receptors' (Table 1). Endostatin is known to associate with integrin $\alpha_5\beta_1$, to anchor protein caveolin-1, and to activate Src *via* a tyrosyl phosphatase-dependent pathway in human ECs [30]. These are in addition to earlier reports that endostatin contains a RGD (Arg-Gly-Asp) sequence and binds to integrins $\alpha_v\beta_3$ and $\alpha_v\beta_5$ [31]. Furthermore, endostatin, as well as angiostatin, increase cytoplasmic Ca^{2+} in ECs immediately following exposure [32].

The crystal structure of endostatin [33] shows the amino acid sequence to be folded into predominantly anti-parallel β-sheet structure, with interspersed extended loops and two short α-helices, as illustrated in Figure 1A. The structure of endostatin is homologous to that of E-selectin [34]. In fact, the entire β-sheet structure of E-selectin is contained within the endostatin structure. Endostatin is highly positively charged, particularly due to the presence of multiple arginine residues and has a high affinity for heparin, which is required for the full activity of the peptide [35].

Tumstatin and tum-5

Recently, the C-terminal globular non-collagenous NC1 domain of the α3 chain of human type IV collagen (α3(IV)NC1) called tumstatin [36], was reported to have anti-angiogenic properties [37]. Aside from its ability to inhibit angiogenesis *in vitro* and *in vivo*, tumstatin also inhibits tumor cell proliferation [37, 38]. Using deletion mutagenesis, Maeshima et al. [37] found that the anti-angiogenic activity of tumstatin appears to be localized

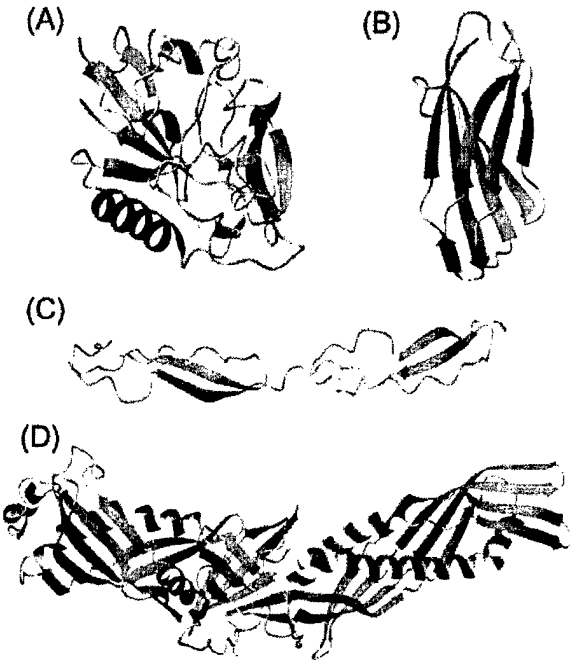

Figure 1. Molecular structures for four anti-angiogenic proteins/peptides. The molecular structures of endostatin [33] (panel 1A), fibronectin type III repeat domain [49] (panel 1B), thrombospondin-1 (TSP-1) [69] (panel 1C), and bactericidal permeability increasing (BPI) protein [91] (panel 1D) are shown. Beta-sheets are shown in blue, helices in red and gray represents random coil and β-turns.

between amino acid residues 54 and 132, a fragment named tum-5, whereas its tumor proliferation inhibitory activity resides between amino acid residues 181 and 244. Maeshima et al. also demonstrated that both tumstatin and tum-5 bind to $\alpha_v\beta_3$ (Table 1) in an RGD-independent manner and that binding is pivotal for anti-angiogenic activity [39]. *In vivo* studies demonstrate that at a molar-equivalent concentration, human tum-5 is at least 10 times more active than human endostatin [40].

PEX

The non-catalytic C-terminal haemopexin-like domain (PEX) of the matrix metalloproteinase MMP-2 can interact with integrin $\alpha_v\beta_3$ to block MMP-2 binding and thereby inhibit angiogenesis. MMPs are mosaic proteins containing an N-terminal pro-domain, a catalytic Zn^{2+} protease domain and the C-terminal PEX haemopexin-like domain. PEX2 appears to be a naturally occurring breakdown product of MMP-2. This protein fragment can inhibit cell-associated collagenolytic activity with preferential substrate specificity towards type IV collagen, which is thought to play an important role in EC proliferation and behaviour during the angiogenic process because it is a major macromolecular constituent of basement membranes [41]. Consequently, PEX inhibits angiogenesis and, in this way, controls normal angiogenesis and neovascularization. Since MMP-2

does not contain the RGD sequence, PEX binding to $\alpha_v\beta_3$ (Table 1) is RGD-independent. Therefore, exogenously administered PEX may be a therapeutic inhibitor of diseases associated with angiogenesis [42] and may be less toxic than treatment with MMP enzyme inhibitors themselves [43].

The structure of the PEX domain in MMP9 is a non-covalent asymmetric homodimer, consisting of multiple β-sheets. The overall structure of PEX9 adopts a four-bladed β-propeller, and blade IV of PEX9 mediates the non-covalent and predominantly hydrophobic dimerization contact [44].

Anastellin

Anastellin is another anti-angiogenic peptide (76 amino acid residues), derived from the first type III repeat of fibronectin [45], which contains a site important in fibronectin self-assembly into fibrils [46]. Anastellin may disrupt intermolecular interactions that maintain fibronectin in its soluble form [46], and this disruption may induce the molecule to undergo assembly into fibrils [45]. Alternatively, anastellin may change the conformation of fibronectin in such a way that cryptic fibronectin–fibronectin binding sites that are capable of driving fibril assembly are exposed. Systemic treatment of tumor-bearing mice with anastellin suppresses the growth of subcutaneous tumors and inhibits tumor angiogenesis, as well as metastasis [47].

This first type III repeat in fibronectin has a similar function as the NC1 domain from collagen IV. This suggests a common mechanism for anti-angiogenic substances derived from extracellular matrix and blood proteins [47], especially considering that these anti-angiogenic substances bind to adhesion molecules containing the RGD-sequence. For instance, angiostatin binds to vitronectin, endostatin binds to fibulins, and nidogen-2 and anastellin bind to fibronectin and fibrinogen in serum [47]. But moreover, all bind to $\alpha_v\beta_3$ (Table 1), which is expressed at high levels in angiogenic ECs [48].

As shown in Figure 1B, the fibronectin type III domain consists of seven β-strands folded into two anti-parallel β-sheets having an immunoglobulin-like fold similar to that found in homologous modules in the cytokine receptor superfamily [49, 50]. Moreover, the surface of this molecule is highly positively charged.

Others

Prolactin, growth hormone and placental lactogen are members of a family of polypeptide hormones that share structural similarities and biological activities. They modulate angiogenesis along with two non-classical members of the family, proliferin and proliferin related protein. Opposing actions have been described between these two similar, yet independent, molecules (proliferin and proliferin related protein), which can stimulate and inhibit angiogenesis, respectively. The potential to exert opposing effects on angiogenesis can also reside within the same molecule as the parent protein promotes angiogenesis (i.e., prolactin, growth hormone and placental lactogen), but after proteolytic processing, the resulting peptide fragment acquires anti-angiogenic properties (i.e., 16 kDa prolactin, 16 kDa growth hormone and 16 kDa placental lactogen) [51–54].

ECs are known to produce various forms of laminin, but the structural characteristics and biological features are incompletely known [55]. Whereas laminin itself, as well as peptides derived from it, are pro-angiogenic [56, 57], vasostatin (residues 1–180 of the NH_2 domain of calreticulin) can bind to laminin, thus promoting anti-angiogenic activity. Calreticulin by itself is anti-angiogenic as well [55]. Domain IVa of the laminin α5 chain is likely to be responsible for the angiogenic response of laminin. This domain promotes cell adhesion and binds to β_1 and $\alpha_v\beta_3$ integrins *via* the RGD sequence [58]. In addition, the laminin receptor 67LR plays an important role in metastasis, tumor invasiveness and tumor angiogenesis because it is upregulated during these conditions. Interestingly, the RDGSYGIV peptide derived from epidermal growth hormone (residues 33–42), which inhibits EC motility, is an antagonist for 67LR [59].

Lastly, the metal-binding glycoprotein osteonectin (also called BM-40 or SPARC) has a protruding N-terminal β-hairpin with striking similarities to epidermal growth factor (EGF) [60]. Although the molecular structure of osteonectin consists mostly of helices, this β-hairpin structure is believed to be the site that promotes anti-angiogenic activity.

Small peptides (<50 amino acid residues)

Identification of anti-angiogenic fragments of proteins that are themselves anti-angiogenic, prompted the search for even smaller anti-angiogenic peptides [61]. This search was motivated by a desire to minimize the therapeutic dosage, to produce the peptide synthetically rather than by using recombinant techniques, to help identify an orally active agent, and, quite simply, to generate new anti-angiogenic compounds. Several approaches were used to achieve this goal: peptide dissection, phage-display, and peptide design. Presented below and listed in Table 2 are examples of some small anti-angiogenic peptides (<50 amino acids) identified using different approaches.

TSP-1 peptides

An extremely potent inhibitor of angiogenesis is thrombospondin-1 (TSP-1), a large modular matrix protein containing three identical disulfide-linked 180 kD chains. TSP-1 is effective at subnanomolar concentrations, both *in vitro* and *in vivo* [62–64] and is secreted at high levels by a variety of normal cells. The use of intact TSP-1 as an anti-angiogenic drug in humans is, however, not practical due to its size (450 kDa) and not

Table 2. Sequences of selected anti-angiogenic peptides.

Name	Sequence	Source
EGF_{33-42}	RDGSYGIV	[59]
Mal II	SPWSSASVTAGDGVITRIR	[65]
7mer	$_{Ac}$-G V I[a] T R I R-$_{Neth}$	[65]
DI-TSP	$_{Ac}$-G V I[a] T Nva I R P-$_{Neth}$	[68]
$PTHrP_{1-10}$	AVSEHQLLHD	[71]
T3	LQRFTTMPFLFCNVNDVCNF	[70]
T7	TMPFLFCNVNDVCNFASRNDYSYWL	[70]
RGD-4C	CDCRGDCFC	[21]
NGR-4C	CNGRCVSGCAGRC	[21]
Flt2-11	NITVTLKKFPL	[78]
Anginex	ANIKLSVQMKLFKRHLK WKIIVKLNDGRELSLD	[20]

[a] The L-amino acid is substituted by the D-enantiomer.

desirable due to its diverse and multiple biological activities. For example, TSP-1 is involved in neurite outgrowth, platelet aggregation, as well as angiogenesis [65]. However, anti-angiogenic peptides derived from native TSP-1 could provide a reasonable alternative.

A central 50-kDa proteolytic fragment of TSP-1 that contains its procollagen homology region and properdin type 1 repeats, retains all of the angiogenesis inhibitory activity of parent TSP-1 [63]. Moreover, TSP-1 repeats (about 60 residues each) have been extensively studied and are known to function as inhibitors of angiogenesis and glycosaminoglycan binding sites (reviewed in [66]). Two peptides, residues 424–442 (Mal I) and residues 481–499 (Mal II) derived from these repeat domains, display anti-angiogenic activity through a CD36-dependent mechanism [63, 67]. However, micro-molar concentrations of the peptides are required to achieve an effect equivalent to that produced by low nanomolar amounts of native TSP-1. This loss of activity could be recovered in one of the peptides, Mal II, by substituting an L-amino acid with its D-isoleucyl enantiomer. Activity was optimized by ethylamide-capping, which resulted in a similar potency to TSP-1 ethylamide-capped heptapeptide [65]. Following further modification to a nonamer containing the non-natural amino acid norvaline (see Table 2), this peptide successfully inhibited tumor growth [68].

The crystal structure of the TSP-1 type 1 repeat [69] (see Figure 1C) contains a three-stranded, anti-parallel β-sheet that consists of alternating stacked layers of tryptophan and arginine residues from respective strands, capped by disulfide bonds on each end. One face of the molecule has a positively charged groove that might be the 'recognition' domain for mediating interactions with various ligands. Peptides derived from these repeats also display β-sheet character when examined by CD spectropolarimetry.

Tumstatin derivatives

As mentioned above, tumstatin (α3(IV)NC1) and its deletion mutant tum-5 (residues 54–132), possess anti-angiogenic activity. To delineate the most active sequence within this 88 residue domain, smaller peptides were synthesized and screened for activity. Two peptides (Table 2): T3 (residues 69–88) and T7 (residues 74–98) were able to inhibit proliferation and to induce apoptosis specifically in ECs. Similar to tumstatin and the tum-5 domain, these peptides bound to and functioned *via* integrin $\alpha_v\beta_3$ in an RGD-independent manner [70]. On a molar basis, peptide T3 was 2- to 5-fold less active than tumstatin or tum-5. Although both peptides have a propensity for β-sheet formation, introduction of a disulfide bond between the two interstrand cysteines present in T3 did not improve activity, as predicted earlier for parent tumstatin [70].

Parathyroid hormone-related peptide

Parathyroid hormone-related peptide (PTHrP) and the closely related parathyroid hormone (PTH) are peptide hormones that regulate serum calcium levels, vascular tone and bone formation [71]. PTHrP is composed of several domains with distinct physiological properties. The first 34 amino acids of PTHrP inhibit angiogenesis, and 5 of the first 10 amino acids in PTH and PTHrP are identical. Moreover, structure predictions indicate that these regions have similar conformations [71]. In human PTH_{1-34}, residues 6–20 and 21–33 fold into two amphiphilic helices that form an overall twisted belt from the N- to the C-termini with the crossing point near residue Arg-20 [72]. The dimer interface is mainly hydrophobic and the mid- and C-terminal portions of the hydrophilic surface are composed primarily of positively charged residues. However, the sequence that promotes anti-angiogenic activity seems to be the ten aperiodic N-terminal residues AVSEHQLLHD [71], and this sequence is predicted to have a high propensity to form β-sheet conformation, which may be 'locked-in' upon binding its receptor.

RGD-based peptides

The overexpression of adhesion molecules such as $\alpha_v\beta_3$, $\alpha_3\beta_5$ and β1-integrins, on ECs of angiogenic blood vessels is generally found to be associated with the angiogenesis process. This observation urged researchers to develop antagonists that block EC interactions with the extracellular matrix as a way to inhibit angiogenesis [48, 73–76]. One natural integrin-binding ligand is the RGD-tripeptide sequence present in numerous endogenous proteins.

Considerable research is being performed to identify other related sequences. One study using *in vivo* selection of phage display peptide libraries to isolate peptides that specifically home to angiogenic (tumor) blood vessels, revealed a number of peptide motifs that specifically bind to tumor vasculature. One of these peptides, RGD-4C {d(CDCRGDCFC)$_2$} is a molecule containing the integrin-binding sequence RGD (Arg-Gly-Asp) (Table 2) [21, 22, 77]. Another peptide, d(CNGRCVSG CAGRC)$_2$, with a $CX_3CX_3CX_3$ structural motif contains

the sequence NGR (Asn-Gly-Arg), known to be another cell adhesion binding motif (Table 2). Phages expressing these peptides specifically home in on angiogenic blood vessels from different tumor types, including carcinomas, sarcomas, melanomas. A third peptide containing the motif GSL (Gly-Ser-Leu) is also frequently recovered from breast carcinoma and Karposi's sarcoma [21].

Flt-1 peptide

Vascular endothelial growth factor (VEGF) is a well-known angiogenic stimulator, which functions through two endothelial specific tyrosine kinase receptors, Flt-1 (VEGFR-1) and Flk-1 (VEGFR-2). Tan et al. [78] demonstrated that an 11 amino acid peptide (Flt2-11; Table 2) derived from the second immunoglobulin domain of Flt-1 functions as an angiogenesis inhibitor by inhibiting VEGF function through a non-VEGF binding mechanism, i.e., without binding to VEGF or inhibiting VEGF's binding to its receptors. Peptide sequences in Flt-1 were identified primarily using Flt-1 VEGF-binding domain data by mutational analysis [79] and the VEGF-Flt-1D2 protein crystal structure [80]. Of the two peptides chosen (SPNITVTLKKFPL and RPFVEMYSEIPE), the former one demonstrated anti-angiogenic activity in the CAM assay, and this activity could be slightly enhanced by removing the N-terminal dipeptide SP.

The crystal structure of the VEGF-Flt-1D2 protein complex indicates that parts of this active peptide are within the third β-sheet of Flt-1D2, and CD and NMR analyses indicate that the NITVTLKKFPL peptide (Flt2-11) in solution forms a stable extended structure, presumably β-strand, that can be stabilized by self-association to a dimer at higher concentrations. In the context of a β-strand conformation, the Flt-1 peptide NITVTLKKFPL would present N-terminal hydrophobic amino acid residues I-V-L on the same face of the strand.

VEGF-binding peptides

Phage display has been used to identify peptides that bind to VEGF and thereby inhibit its angiogenic activity. By using this approach, Fairbrother et al. [81] identified a number of VEGF-binding peptides, and Pan et al. [82] reported the NMR structure of one of these peptides, a 19mer, that has a turn-helix conformation with hydrophobic residues partitioned to one face of the folded peptide and polar/charged residues at the other face. Binding to the VEGF dimer is promoted *via* interactions with hydrophobic residues.

Anginex

As discussed above, most anti-angiogenic agents are endogenous molecules or derived from endogenous molecules, primarily proteins. On the other hand, Griffioen et al. [20] reported the potent anti-angiogenic activity of a designed peptide 33mer [83], called anginex or βpep-25. Anginex specifically targets angiogenically activated ECs, inhibiting EC adhesion to and migration on the extracellular matrix and thereby inducing apoptosis. Although no specific receptor for anginex has yet been identified, it appears that one or more adhesion/migration receptor(s), upregulated in angiogenically activated ECs, is (are) involved [20]. In tumor models in mice, anginex is highly effective at inhibiting tumor growth [84–86].

NMR structural studies show that anginex folds amphipathically into a three-stranded anti-parallel β-sheet motif [87]. The hydrophilic face of the folded peptide carries a high net positive charge (+5), mostly from lysine residues. This fold and composition is similar to that found in a number of other β-sheet-structured, anti-angiogenic cytokines, such as TNF [88], lymphotoxin (LT or TNF-β) [89], transforming growth factor-β (TGF-β) [90], and bactericidal/permeability increasing protein (BPI) [91, 92]. The structure of BPI is shown in Figure 1D to illustrate the extent of its β-sheet fold. Although anginex contains a short β-strand sequence identical to one from BPI, that same synthetic sequence from BPI demonstrates no anti-angiogenic activity, indicating that it is the unique anginex sequence and fold that impart anti-angiogenic function.

Structural similarities among anti-angiogenic proteins/peptides

Considering protein fragments and peptides discussed above, it should be apparent that aside from their functional commonality of being anti-angiogenic, these peptides, for the most part, are also structurally and compositionally similar. The vast majority folds as anti-parallel β-sheets and contain a relatively high incidence of hydrophobic and cationic residues.

In general, for smaller derived peptides (Table 2), the same can be said. Because experimentally determined structures are not available for all these peptides, the program PSIPRED was used to assess folding potential. The secondary structures of all these smaller peptides are predicted to also exist in β-strand conformation. Although these sequences are compositionally similar, sequence alignment analysis using several homology programs did not indicate significant sequential commonalties among these peptides.

In addition, many other anti-angiogenic proteins, e.g. PF4 [93], TNF [88] and BPI [91], are also structurally and compositionally similar to protein fragments and smaller peptides discussed above. Although the significance of this correlation is unclear, it appears that the mechanisms of action of these anti-angiogenics are not the same, i.e., they function using different receptors. Few receptors reported to mediate the signal leading to angiostasis are definitive. In fact, the picture in terms of receptors is quite untransparent and a number of these

agents apparently can act on multiple receptors (see Table 1). For example, ATP-synthase on ECs has been reported to be a receptor for angiostatin [25]. However, other angiostatin receptors include $\alpha_v\beta_3$ and, to a lesser extent, $\alpha_9\beta_1$ [24]. Karumanchi et al. [94] demonstrated the existence of a low affinity cell surface glypican receptor for endostatin, along with a yet-to-be-identified high affinity receptor, and a third intercellular protein, an epitope (hTM3) in tropomyosin, was also found to bind endostatin [95]. Another such example is TSP-1, which requires, both *in vitro* [67] and *in vivo* [96], the expression of the transmembrane receptor CD36 as the receptor for TSP-1. TSP-1 is also known to bind to other receptors, such as Syndecan, heparin sulfate proteoglycans (HSPG) and integrin associate protein (IAP) (reviewed in [66]). The presence of multiple receptors, although possibly being therapeutically beneficial, complicates our understanding of tumor angiogenesis and our ability to develop receptor-specific antagonists.

The compositional and structural similarity noted among these anti-angiogenic peptides may be used, possibly *via* combinatorial approaches, to design additional therapeutic anti-angiogenic agents. In the context of a β-strand conformation, for example, the Flt-1 peptide NITVTLKKFPL would present N-terminal hydrophobic amino acid residues I-V-L on the same face of the strand. This presentation pattern is observed in a number of anti-angiogenic peptides. In fact, anginex shows the same β-strand I-V-L pattern, as well as the cross-strand pattern, V-M-L. Because anginex, for example, forms β-sheet structure and can be used as a presentation scaffold, it might be possible to vary a set number of residues and make analogs having various permutations and combinations of amino acid residues. In this way, one might optimize angiostatic potential. In addition, it might be possible to reduce the size of the active peptide, which could help lead to the design of an actual small molecule mimetic of an anti-angiogenic peptide.

Conclusions

As more anti-angiogenic peptides are identified, it is becoming apparent that there are compositional and structural similarities that may well act to convey bioactivity. These peptides have a high incidence of hydrophobic residues, are primarily cationic in nature and fold as anti-parallel β-sheets. Aside from the fact that small peptide inhibitors have various advantages over larger anti-angiogenic agents, they may also be used to help design better, more active anti-angiogenic peptides or even small molecule mimetics.

Acknowledgements

This research was supported by grants from the Dutch Cancer Society (to A.W. Griffioen), the Department of Defense DA/DAMD 17-99-1-9564 (to K. H. Mayo) and the National Institutes of Health R01 CA-96090 (to K. H. Mayo).

References

1. Folkman J. Tumor angiogenesis: Therapeutic implications. N Engl J Med 1971; 285: 1182–6.
2. Folkman J. Anti-angiogenesis: New concept for therapy of solid tumors. Ann Surg 1972; 175: 409–16.
3. O'Reilly MS, Holmgren L, Shing Y et al. Angiostatin: A novel angiogenesis inhibitor that mediates the suppression of metastases by a Lewis lung carcinoma. Cell 1994; 79: 315–28.
4. O'Reilly MS, Boehm T, Shing Y et al. Endostatin: An endogenous inhibitor of angiogenesis and tumor growth. Cell 1997; 88: 277–85.
5. Fogarty M. Learning from Angiogenesis Trial Failures. Scientist 2002; 16: 33–5.
6. Hansen-Algenstaedt N, Fukumura D, Stoll B et al. Second wave of angiogenesis during KDR/flk-1 antibody therapy [abstract]. Proc Am Assoc Cancer Res 1999; 40: 620.
7. Hull C, McLean G, Wong F et al. Lipopolysaccharide signals an endothelial apoptosis pathway through TNF receptor-associated factor 6-mediated activation of c-Jun NH2-terminal kinase. J Immunol 2002; 169: 2611–8.
8. Guida E, Stewart A. Influence of hypoxia and glucose deprivation on tumour necrosis factor-alpha and granulocyte-macrophage colony-stimulating factor expression in human cultured monocytes. Cell Physiol Biochem 1998; 8: 75–88.
9. Bornstein P, Armstrong LC, Hankenson KD et al. Thrombospondin 2, a matricellular protein with diverse functions. Matrix Biol 2000; 19: 557–68.
10. Kyriakides TR, Zhu YH, Smith LT et al. Mice that lack thrombospondin 2 display connective tissue abnormalities that are associated with disordered collagen fibrillogenesis, an increased vascular density, and a bleeding diathesis. J Cell Biol 1998; 140: 419–30.
11. Armstrong LC, Bjorkblom B, Hankenson KD et al. Thrombospondin 2 inhibits microvascular endothelial cell proliferation by a caspase-independent mechanism. Mol Biol Cell 2002; 13: 1893–905.
12. Kong HL, Crystal RG. Gene therapy strategies for tumor antiangiogenesis. J Natl Cancer Inst 1998; 90: 273–86.
13. Derbyshire EJ, Thorpe PE. Targeting the tumor endothelium using specific antibodies. In RL Be (ed.): Tumor Angiogenesis. Oxford: Oxford University Press 1997; 343–56.
14. Hansen-Algenstaedt N, Stoll BR, Padera TP et al. Tumor oxygenation in hormone-dependent tumors during vascular endothelial growth factor receptor-2 blockade, hormone ablation, and chemotherapy. Cancer Res 2000; 60: 4556–60.
15. Wang Y, Becker D. Antisense targeting of basic fibroblast growth factor and fibroblast growth factor receptor-1 in human melanomas blocks intratumoral angiogenesis and tumor growth. Nat Med 1997; 3: 887–93.
16. Lin P, Sankar S, Shan S et al. Inhibition of tumor growth by targeting tumor endothelium using a soluble vascular endothelial growth factor receptor. Cell Growth Differ 1998; 9: 49–58.
17. Fong TA, Shawver LK, Sun L et al. SU5416 is a potent and selective inhibitor of the vascular endothelial growth factor receptor (Flk-1/KDR) that inhibits tyrosine kinase catalysis, tumor vascularization, and growth of multiple tumor types. Cancer Res 1999; 59: 99–106.
18. Ke LD, Fueyo J, Chen X et al. A novel approach to glioma gene therapy: Down-regulation of the vascular endothelial growth factor in glioma cells using ribozymes. Int J Oncol 1998; 12: 1391–6.
19. Hamby JM, Showalter HD. Small molecule inhibitors of tumor-promoted angiogenesis, including protein tyrosine kinase inhibitors. Pharmacol Ther 1999; 82: 169–93.

20. Griffioen AW, van der Schaft DW, Barendsz-Janson AF et al. Anginex, a designed peptide that inhibits angiogenesis. Biochem J 2001; 354: 233–42.
21. Arap W, Pasqualini R, Ruoslahti E. Cancer treatment by targeted drug delivery to tumor vasculature in a mouse model. Science 1998; 279: 377–80.
22. Pasqualini R, Koivunen E, Ruoslahti E. Alpha v integrins as receptors for tumor targeting by circulating ligands. Nat Biotechnol 1997; 15: 542–6.
23. Cao Y, Ji RW, Davidson D et al. Kringle domains of human angiostatin. Characterization of the anti-proliferative activity on endothelial cells. J Biol Chem 1996; 271: 29461–7.
24. Tarui T, Miles LA, Takada Y. Specific interaction of angiostatin with integrin alpha(v)beta(3) in endothelial cells. J Biol Chem 2001; 276: 39562–8.
25. Moser TL, Stack MS, Asplin I et al. Angiostatin binds ATP synthase on the surface of human endothelial cells. Proc Natl Acad Sci USA 1999; 96: 2811–6.
26. Cao Y, Chen A, An SS et al. Kringle 5 of plasminogen is a novel inhibitor of endothelial cell growth. J Biol Chem 1997; 272: 22924–8.
27. Abad MC, Arni RK, Grella DK et al. The X-ray crystallographic structure of the angiogenesis inhibitor angiostatin. J Mol Biol 2002; 318: 1009–17.
28. Oh SP, Kamagata Y, Muragaki Y et al. Isolation and sequencing of cDNAs for proteins with multiple domains of Gly-Xaa-Yaa repeats identify a distinct family of collagenous proteins. Proc Natl Acad Sci USA 1994; 10: 4229–33.
29. Ramchandran R, Dhanabal M, Volk R et al. Antiangiogenic activity of restin, NC10 domain of human collagen XV: Comparison to endostatin. Biochem Biophys Res Commun 1999; 255: 735–9.
30. Wickstrom SA, Alitalo K, Keski-Oja J. Endostatin associates with integrin alpha5beta1 and caveolin-1, and activates Src via a tyrosyl phosphatase-dependent pathway in human endothelial cells. Cancer Res 2002; 62: 5580–9.
31. Rehn M, Veikkola T, Kukk-Valdre E et al. Interaction of endostatin with integrins implicated in angiogenesis. Proc Natl Acad Sci USA 2001; 98: 1024–9.
32. Jiang L, Jha V, Dhanabal M et al. Intracellular Ca(2+) signaling in endothelial cells by the angiogenesis inhibitors endostatin and angiostatin. Am J Physiol 2001; 280: C1140–50.
33. Hohenester E, Sasaki T, Olsen BR, Timpl R. Crystal structure of the angiogenesis inhibitor endostatin at 1.5 A resolution. EMBO J 1998; 17: 1656–64.
34. Graves BJ, Crowther RL, Chandran C et al. Insight into E-selectin/ligand interaction from the crystal structure and mutagenesis of the lec/EGF domains. Nature 1994; 367: 532–8.
35. Dixelius J, Larsson H, Sasaki T et al. Endostatin-induced tyrosine kinase signaling through the Shb adaptor protein regulates endothelial cell apoptosis. Blood 2000; 95: 3403–11.
36. Timpl R, Wiedemann H, van Delden V et al. A network model for the organization of type IV collagen molecules in basement membranes. Eur J Biochem 1981; 120: 203–11.
37. Maeshima Y, Colorado PC, Torre A et al. Distinct antitumor properties of a type IV collagen domain derived from basement membrane. J Biol Chem 2000; 275: 21340–8.
38. Han J, Ohno N, Pasco S et al. A cell binding domain from the alpha3 chain of type IV collagen inhibits proliferation of melanoma cells. J Biol Chem 1997; 272: 20395–401.
39. Maeshima Y, Colorado PC, Kalluri R. Two RGD-independent alpha vbeta 3 integrin binding sites on tumstatin regulate distinct anti-tumor properties. J Biol Chem 2000; 275: 23745–50.
40. Maeshima Y, Manfredi M, Reimer C et al. Identification of the anti-angiogenic site within vascular basement membrane-derived tumstatin. J Biol Chem 2001; 276: 15240–8.
41. Madri JA. Extracellular matrix modulation of vascular cell behaviour. Transpl Immunol 1997; 5: 179–83.
42. Brooks PC, Silletti S, von Schalscha TL et al. Disruption of angiogenesis by PEX, a noncatalytic metalloproteinase fragment with integrin binding activity. Cell 1998; 92: 391–400.
43. Hughes S. Bayer drug casts shadow over MMP inhibitors in cancer. SCRIP 1999; 20: 2477.
44. Cha H, Kopetzki E, Huber R et al. Structural basis of the adaptive molecular recognition by MMP9. J Mol Biol 2002; 320: 1065–79.
45. Morla A, Zhang Z, Ruoslahti E. Superfibronectin is a functionally distinct form of fibronectin. Nature 1994; 367: 193–6.
46. Morla A, Ruoslahti E. A fibronectin self-assembly site involved in fibronectin matrix assembly: Reconstruction in a synthetic peptide. J Cell Biol 1992; 118: 421–9.
47. Yi M, Ruoslahti E. A fibronectin fragment inhibits tumor growth, angiogenesis, and metastasis. Proc Natl Acad Sci USA 2001; 98: 620–4.
48. Brooks PC, Clark RA, Cheresh DA. Requirement of vascular integrin alpha v beta 3 for angiogenesis. Science 1994; 264: 569–71.
49. Baron M, Main AL, Driscoll PC et al. 1H NMR assignment and secondary structure of the cell adhesion type III module of fibronectin. Biochemistry 1992; 31: 2068–73.
50. Leahy DJ, Hendrickson WA, Aukhil I, Erickson HP. Structure of a fibronectin type III domain from tenascin phased by MAD analysis of the selenomethionyl protein. Science 1992; 258: 987–91.
51. Ferrara N, Clapp C, Weiner R. The 16K fragment of prolactin specifically inhibits basal or fibroblast growth factor stimulated growth of capillary endothelial cells. Endocrinology 1991; 129: 896–900.
52. Corbacho AM, Martinez De La Escalera G, Clapp C. Roles of prolactin and related members of the prolactin/growth hormone/placental lactogen family in angiogenesis. J Endocrinol 2002; 173: 219–38.
53. Nelson J, Scott WN, Allen WE et al. Murine epidermal growth factor peptide (33–42) binds to a YIGSR-specific laminin receptor on both tumor and endothelial cells. J Biol Chem 1996; 271: 26179–86.
54. Struman I, Bentzien F, Lee H et al. Opposing actions of intact and N-terminal fragments of the human prolactin/growth hormone family members on angiogenesis: An efficient mechanism for the regulation of angiogenesis. Proc Natl Acad Sci USA 1999; 96: 1246–51.
55. Yao L, Pike SE, Tosato G. Laminin binding to the calreticulin fragment vasostatin regulates endothelial cell function. J Leukoc Biol 2002; 71: 47–53.
56. Malinda KM, Nomizu M, Chung M et al. Identification of laminin alpha1 and beta1 chain peptides active for endothelial cell adhesion, tube formation, and aortic sprouting. Faseb J 1999; 13: 53–62.
57. Grant DS, Tashiro K, Segui-Real B et al. Two different laminin domains mediate the differentiation of human endothelial cells into capillary-like structures *in vitro*. Cell 1989; 58: 933–43.
58. Sasaki T, Timpl R. Domain IVa of laminin alpha5 chain is cell-adhesive and binds beta1 and alphaVbeta3 integrins through Arg-Gly-Asp. FEBS Lett 2001; 509: 181–5.
59. Gebarowska D, Stitt AW, Gardiner TA et al. Synthetic peptides interacting with the 67-kd laminin receptor can reduce retinal ischemia and inhibit hypoxia-induced retinal neovascularization. Am J Pathol 2002; 160: 307–13.
60. Hohenester E, Maurer P, Timpl R. Crystal structure of a pair of follistatin-like and EF-hand calcium-binding domains in BM-40. Embo J 1997; 16: 3778–86.
61. Cao Y, Cao R, Brakenhielm E. Antiangiogenic mechanisms of diet-derived polyphenols. J Nutr Biochem 2002; 13: 380–90.
62. Good DJ, Polverini PJ, Rastinejad F et al. A tumor suppressor-dependent inhibitor of angiogenesis is immunologically and functionally indistinguishable from a fragment of thrombospondin. Proc Natl Acad Sci USA 1990; 87: 6624–8.
63. Tolsma SS, Volpert OV, Good DJ et al. Peptides derived from two separate domains of the matrix protein thrombospondin-1 have anti-angiogenic activity. J Cell Biol 1993; 122: 497–511.
64. Adragna NC, Fonseca P, Lauf PK. Hydroxyurea affects cell morphology, cation transport, and red blood cell adhesion in cultured vascular endothelial cells. Blood 1994; 83: 553–60.

65. Dawson DW, Volpert OV, Pearce SF et al. Three distinct D-amino acid substitutions confer potent antiangiogenic activity on an inactive peptide derived from a thrombospondin-1 type 1 repeat. Mol Pharmacol 1999; 55: 332–8.
66. Chen H, Herndon ME, Lawler J. The cell biology of thrombospondin-1. Matrix Biol 2000; 19: 597–614.
67. Dawson DW, Pearce SF, Zhong R et al. CD36 mediates the *In vitro* inhibitory effects of thrombospondin-1 on endothelial cells. J Cell Biol 1997; 138: 707–17.
68. Reiher FK, Volpert OV, Jimenez B et al. Inhibition of tumor growth by systemic treatment with thrombospondin-1 peptide mimetics. Int J Cancer 2002; 98: 682–9.
69. Tan K, Duquette M, Liu JH et al. Crystal structure of the TSP-1 type 1 repeats: A novel layered fold and its biological implication. J Cell Biol 2002; 159: 373–82.
70. Maeshima Y, Yerramalla UL, Dhanabal M et al. Extracellular matrix-derived peptide binds to alpha(v)beta(3) integrin and inhibits angiogenesis. J Biol Chem 2001; 276: 31959–68.
71. Bakre MM, Zhu Y, Yin H et al. Parathyroid hormone-related peptide is a naturally occurring, protein kinase A-dependent angiogenesis inhibitor. Nat Med 2002; 8: 995–1003.
72. Jin L, Briggs SL, Chandrasekhar S et al. Crystal structure of human parathyroid hormone 1–34 at 0.9-A resolution. J Biol Chem 2000; 275: 27238–44.
73. Brooks PC, Montgomery AM, Rosenfeld M et al. Integrin alpha v beta 3 antagonists promote tumor regression by inducing apoptosis of angiogenic blood vessels. Cell 1994; 79: 1157–64.
74. Friedlander M, Brooks PC, Shaffer RW et al. Definition of two angiogenic pathways by distinct alpha v integrins. Science 1995; 270: 1500–2.
75. Fukazawa H, Yoshida K, Ichinohasama R et al. Expression of the Hermes-1 (CD44) and ICAM-1 (CD54) molecule on the surface of thyroid cells from patients with Graves' disease. Thyroid 1993; 3: 285–9.
76. Jonjic N, Alberti S, Bernasconi S et al. Heterogeneous susceptibility of human melanoma clones to monocyte cytotoxicity: Role of ICAM-1 defined by antibody blocking and gene transfer. Eur J Immunol 1992; 22: 2255–60.
77. Sgadari C, Angiolillo AL, Tosato G. Inhibition of angiogenesis by interleukin-12 is mediated by the interferon-inducible protein 10. Blood 1996; 87: 3877–82.
78. Tan DC, Kini RM, Jois SD et al. A small peptide derived from Flt-1 (VEGFR-1) functions as an angiogenic inhibitor. FEBS Lett 2001; 494: 150–6.
79. Davis-Smyth T, Chen H, Park J et al. The second immunoglobulin-like domain of the VEGF tyrosine kinase receptor Flt-1 determines ligand binding and may initiate a signal transduction cascade. Embo J 1996; 15: 4919–27.
80. Wiesmann C, Fuh G, Christinger HW et al. Crystal structure at 1.7 A resolution of VEGF in complex with domain 2 of the Flt-1 receptor. Cell 1997; 91: 695–704.
81. Fairbrother WJ, Christinger HW, Cochran AG et al. Novel peptides selected to bind vascular endothelial growth factor target the receptor-binding site. Biochemistry 1998; 37: 17754–64.
82. Pan B, Li B, Russell SJ et al. Solution structure of a phage-derived peptide antagonist in complex with vascular endothelial growth factor. J Mol Biol 2002; 316: 769–87.
83. Mayo KH, Ilyina E, Park H. A recipe for designing water-soluble, beta-sheet-forming peptides. Protein Sci 1996; 5: 13001–15.
84. Van Der Schaft DW, Dings RP, De Lussanet QG et al. The designer antiangiogenic peptide anginex targets tumor endothelial cells and inhibits tumor growth in animal models. Faseb J 2002; 16: 1991–3.
85. Dings RPM, Yokoyama Y, Ramakrishnan S et al. The designed angiostatic peptide anginex synergistically improves chemotherapy and antiangiogenesis therapy with angiostatin. Cancer Res, in press.
86. Dings RPM, van der Schaft DW, Hargittai B et al. Anti-tumor activity of the novel angiogenesis inhibitor anginex. Can Lett, in press.
87. Ilyina E, Roongta V, Mayo KH. NMR structure of a de novo designed, peptide 33mer with two distinct, compact beta-sheet folds. Biochemistry 1997; 36: 5245–50.
88. Jones EY, Stuart DI, Walker NP. Structure of tumour necrosis factor. Nature 1989; 338: 225–8.
89. Eck MJ, Ultsch M, Rinderknecht E et al. The structure of human lymphotoxin (tumor necrosis factor-beta) at 1.9-A resolution. J Biol Chem 1992; 267: 2119–22.
90. Daopin S, Piez KA, Ogawa Y, Davies DR. Crystal structure of transforming growth factor-beta 2: An unusual fold for the superfamily. Science 1992; 257: 369–73.
91. Beamer LJ, Carroll SF, Eisenberg D. Crystal structure of human BPI and two bound phospholipids at 2.4 angstrom resolution. Science 1997; 276: 1861–4.
92. van der Schaft DW, Toebes EA, Haseman JR et al. Bactericidal/permeability-increasing protein (BPI) inhibits angiogenesis via induction of apoptosis in vascular endothelial cells. Blood 2000; 96: 176–81.
93. Mayo KH, Roongta V, Ilyina E et al. NMR solution structure of the 32-kDa platelet factor 4 ELR-motif N-terminal chimera: A symmetric tetramer. Biochemistry 1995; 34: 11399–409.
94. Karumanchi SA, Jha V, Ramchandran R et al. Cell surface glypicans are low-affinity endostatin receptors. Mol Cell 2001; 7: 811–22.
95. MacDonald NJ, Shivers WY, Narum DL et al. Endostatin binds tropomyosin. A potential modulator of the antitumor activity of endostatin. J Biol Chem 2001; 276: 25190–6.
96. Jimenez B, Volpert OV, Crawford SE et al. Signals leading to apoptosis-dependent inhibition of neovascularization by thrombospondin-1. Nat Med 2000; 6: 41–8.

Version: *in press*
For: *JBC*
File: Mayo et al.doc/PDF

Design of a partial-peptide mimetic of anginex with antiangiogenic and anticancer activity

Kevin H. Mayo[*,†,¥], Ruud P.M. Dings[*,§], Carolee Flader[¶], Irina Nesmelova[*], Balasz Hargittai[*], Daisy W.J. van der Schaft[§], Loes I. van Eijk[§], Dinesha Walek[*], Judy Haseman[*], Thomas R. Hoye[¶], and Arjan W. Griffioen[§]

Departments of Biochemistry, Molecular Biology & Biophysics[*] and Chemistry[¶], University of Minnesota, Minneapolis, Minnesota 55455, and the Angiogenesis Laboratory[§], Research Institute for Growth & Development, Depts. of Pathology and Internal Medicine, University Hospital Maastricht, 6202 AZ Maastricht, The Netherlands

running title: **Designer peptide mimetic inhibits tumor growth**

[†]To whom correspondence should be addressed:
Dr. K. H. Mayo, Dept. of Biochemistry, 6-155 Jackson Hall, University of Minnesota Health Sciences Center, 321 Church Street, Minneapolis, Minnesota 55455, USA, Phone: 612-625-9968; Fax: 612-624-5121; E-mail: mayox001@tc.umn.edu.
[¥]The author has a financial interest in ActiPep Biotechnology, Inc., which holds license to commercialize pharmaceutical agents discussed in this article.

Number of text pages: 21
Number of figures: 4
Number of tables: 3

Key words: ß-sheet structure, angiogenesis, apoptosis, endothelium and cytokines.

Based on structure-activity relationships of the angiostatic ß-sheet-forming peptide anginex, we have designed a mimetic, 6DBF7, which inhibits angiogenesis and tumor growth in mice. 6DBF7 is composed of a ß-sheet-inducing dibenzofuran (DBF) turn-mimetic and two short key amino acid sequences from anginex. This novel antiangiogenic molecule is more effective *in vivo* than parent anginex. In a mouse xenograft model for ovarian carcinoma, 6DBF7 is observed to reduce tumor growth by up to 80%. It is suggested that the activity is based on antiangiogenesis because *in vitro* tube formation is inhibited and because treatment of tumor-bearing mice led to a significant reduction in microvessel density within the tumor. This partial peptide-mimetic is the first EC-specific molecule designed as a substitute for an angiostatic inhibitory peptide.

Angiogenesis, the process of new blood vessel formation, is key to normal organ development, as well as to various pathological disorders like cancer, arthritis, diabetic retinopathy and restenosis (1). The use of agents that can inhibit angiogenesis, particularly in anti-tumor research e.g. (2,3), has indicated that antiangiogenic therapy can be a promising therapeutic modality in the future. To date, the search for angiogenesis inhibitors has been focused on controlling two of the processes that promote angiogenesis: endothelial cell (EC)* growth and EC adhesion (4,5). Targeting EC as anti-tumor treatment is attractive primarily because EC are more accessible than are other cells to pharmacologic agents delivered via the blood, and EC are genetically stable and are not easily mutated into drug resistant variants. Most antiangiogenic agents have been discovered by identifying endogenous molecules, primarily proteins, that inhibit EC growth. This traditional approach has produced a number of antiangiogenics, such as platelet factor-4 (PF4) (6), thrombospondin (7), interferon-γ inducible protein-10 (8), angiostatin (9), endostatin and restin (2,10) and bactericidal-permeability increasing (BPI) protein (11).

Numerous angiostatic compounds have been identified, many of which are currently in various phases of clinical cancer trials (http://cancertrials.nci.nih.gov). Although a number of compounds have shown promise in the clinic, no major breakthroughs have been reported using antiangiogenic agents as stand-alone therapy. This underscores the need for more and better angiostatic compounds for use as stand-alone or in combination with conventional therapies. Moreover, some angiogenesis inhibitors have been shown to be ineffective or to cause diverse

and multiple unwanted biological side-effects (12). This latter phenomemon was, to some extent, expected as many of these endogenous angiostatic proteins are pleiotropic, i.e., they are involved in several biological processes. Often these functions are found to arise from separate sites on the molecule and thus can be separated using smaller segments or domains of a given protein (13). This relates to the search for new antiangiogenic agents, which is aimed at improving specificity, reducing the therapeutic dosage, and minimizing molecular size with a small molecule antiangiogenic agent or antiangiogenic protein mimetic. This is one of the main goals among structural biologists and pharmaceutical chemists working to produce novel antiangiogenic agents. For the design of small molecule mimetics of antiangiogenic proteins, the identification of specific, functionally key amino acid residues and their spatial relationships is crucial. Nevertheless, structure-activity relationships (SARs) for antiangiogenic proteins are sorely needed, and even the analysis of high-resolution molecular structures of a number of antiangiogenic proteins, e.g., endostatin (14), PF4 (15) and BPI (16), has yet to provide this information.

Recently, we reported the design of the anginex peptide, a cytokine-like ß-sheet-forming peptide 33mer (17), which is a potent inhibitor of angiogenesis (1) and tumor growth (18-20). Anginex is more effective at inhibiting EC growth than platelet factor-4 and several other well-known angiogenesis inhibitors such as angiostatin, endostatin, AGM-1470 and thrombospondin-1 (1)*. This peptide 33mer acts by specifically blocking adhesion and migration of angiogenically-activated EC, leading to apoptosis and ultimately to inhibition of angiogenesis *in vitro* and *in vivo* and inhibition of human tumor growth by up to about 80% in various models (18-20). Anginex is an amphipathic ß-sheet-forming peptide (17,21), and because of anginex's relatively small size, a complete SAR is easier to perform than with larger known antiangiogenic proteins like those mentioned above. Here, we report for the first time the design of a partial-peptide mimetic of anginex that was based on the identification of functionally key residues and the conformation responsible for anginex's antiangiogenic activity.

MATHERIALS AND METHODS

Peptide Synthesis—Peptides were synthesized using a Milligen/Biosearch 9600 peptide solid-phase synthesizer using fluorenylmethoxycarbonyl (Fmoc) chemistry. Lyophilized crude peptides were purified by preparative reversed-phase HPLC on a C18 column with an elution gradient of 0-60% acetonitrile with 0.1% trifluoroacetic acid in water. The purity and composition of the peptides were verified by HPLC (Beckman Model 6300) analysis of amino acid composition of hydrolysates prepared by treating the peptides under argon in 6 N HCl for 24 hours at 110 °C. The amino acid sequences of peptides were confirmed by N-terminal sequencing and mass spectrometry.

Synthesis of DBF analogs—Unexceptional phases of solid-phase peptide synthesis (SPPS) were carried out on an ABI (Applied Biosystems, Inc.) 431 peptide synthesizer using Fmoc methodology and BOP/HOBT as coupling reagents. Fmoc-DBF-CO_2H (**1**) was prepared by slight modification of the reported method (22). In this nine-step synthesis, the intermediates and final product were characterized by TLC and ^1H NMR, with GC-LRMS, ^{13}C NMR, mp, and IR being used as appropriate. Coupling of **1** to I20 as well as of L11 to the peptide-DBF-NH_2 was performed on the synthesizer. Coupling of Fmoc-K10-CO_2H to the peptide-DBF-L11-NH_2 sequence was difficult and required manual SPPS using the more reactive HATU reagent (23). The remaining couplings required for production of 2DBF7 through 11DBF7 were carried out using BOP/HOBT conditions on the peptide synthesizer. After the final Fmoc deprotection, each of the DBF peptides was released from the resin with simultaneous removal of all acidolyzable trityl and *tert*-butyl side-chain protecting groups using Reagent K (24). A Rink amide or similar resin was used to provide the primary amide form of the C-terminal D24 unit. Lyophilized crude peptides were purified by HPLC as described above. Purity and composition of the peptides were verified by analytical HPLC, matrix assisted laser desorption ionization (MALDI) mass spectrometry using a Hewlett-Packard G2025A system and sinapinic acid as matrix, and analysis of amino acid composition of hydrolysates (6N HCl, 110 °C, 24 h, under argon).

NMR spectroscopy— For NMR measurements, freeze-dried DBF analogs were dissolved in water-DMSO-DPC mixture. Peptide concentration was 3 mM. pH was adjusted to pH 5.7 by adding μL quantities of NaOD or HCl to the peptide sample. NMR spectra were acquired on a Varian UNITY Plus-600 NMR spectrometer at 25 °C.

2D-homonuclear TOCSY with DIPSI (25) spinlock (mixing time 80 ms) was used to identify spin systems. 2D NOESY experiments (26) were performed for sequential assignments and conformational analysis. WATERGATE (27,28) was used to attenuate the water resonance. Spectra were collected as 256 to 512 t1 experiments, each with 2048 complex data points over a spectral width of 6 kHz in both dimensions with the carrier placed on the water resonance. 16 scans were time averaged per t1 experiment. Data were processed directly on the spectrometer using VNMR (Varian, Inc., Palo Alto) or NMRPipe (29) on an SGI workstation.

Structural modeling—Analysis of NOE growth curves indicated that backbone to backbone inter-proton NOEs were normally maximum at about 200 ms. Interproton distance constraints were derived from NOEs assigned in ^{1}H NOESY spectra acquired with mixing times of 100 ms. NOEs were classified as strong, medium, weak or very weak corresponding to upper bound distance constraints of 2.3, 2.8, 3.5, and 4.5 Å, respectively. The lower bound restraint between non-bonded protons was set to 1.8 Å. Pseudo-atom corrections were added to the upper bound distance constraints where appropriate, and a 0.5 Å correction was added to the upper bound for NOEs involving methyl protons. Hydrogen bond constraints were identified from the pattern of sequential and interstrand NOEs involving NH and C_αH protons, together with evidence of slow amide proton-solvent exchange. Each hydrogen bond identified was defined using two distance constraints; $r_{NH\text{-}0}$ = 1.8 to 2.5 Å, and $r_{N\text{-}0}$ = 1.8 to 2.5 Å.

Derived internuclear distance constraints were used in calculating structures for 6DBF7 by using X-PLOR (30). The molecule was created and a template coordinate set was generated by using the *Template* routine. The *ab initio* simulated annealing (SA) protocol was then used. The SA procedure ran high temperature dynamics (3000 K for 120 ps) and then cooled down to 100 K in 50 K steps with 1.5 ps molecular dynamics at each step. Powell minimization was performed at 100 K for 1000 steps. Structure refinement was done based on simulated annealing starting at 1000 K and ending at 100 K. Final structures were subjected to the X-PLOR Accept

routine with the violation threshold for NOEs of 0.5Å and dihedral angles of 5°. Angles, bond lengths or impropers were not allowed to deviate from ideal geometry more than 5°, 0.05 Å and 5°, respectively. Structures were superimposed using the BIOSYM INSIGHT viewer (Molecular Simulations, Inc.) and were analyzed using X-PLOR analysis routines.

Cells, cultures and reagents—Human umbilical vein derived EC (HUVEC) were harvested from normal human umbilical cords by perfusion with 0.125% trypsin/EDTA. Harvested HUVECs were cultured in gelatin coated tissue culture flasks and subcultured 1: 3 once a week in culture medium (RPMI-1640 with 20% human serum (HS), supplemented with 2 mM glutamine and 100 U/ml penicillin and 0,1 mg/ml streptomycin). Bovine capillary EC (BCE) were kindly provided by Dr. M. Furie (State University of New York, Stony Brook, USA) and were cultured in fibronectin coated tissue culture flasks in RPMI-1640 medium containing 10% FCS, glutamine and antibiotics.

Proliferation measurement—EC proliferation was measured using a [^{3}H]- thymidine incorporation assay. Proliferation of bFGF-stimulated (10 ng/ml) human umbilical vascular EC (HUVEC) cultures was measured by quantification of ^{3}H-thymidine incorporation. Proliferation is expressed as mean counts per minute (cpm) of quadruplicate cultures in three independent experiments (± SEM). EC were seeded at 5000 cells/well in flat-bottomed tissue culture plates and grown for 3 days in the absence or presence of regulators, in culture medium. During the last 6 hours of the assay, the culture was pulsed with 0.5 μCi [methyl-^{3}H]- thymidine/well. Human umbilical vein derived EC (HUVEC) were harvested from normal human umbilical cords by perfusion with 0.125% trypsin/EDTA. Harvested HUVECs were cultured in gelatin coated tissue culture flasks and subcultured 1: 3 once a week in culture medium (RPMI-1640 with 20% human serum (HS), supplemented with 2 mM glutamine and 100 U/mL penicillin and 0.1 mg/mL streptomycin).

In vitro angiogenesis assay—Sprouting and tube formation of bovine EC (BCE) were studied using cytodex-3 beads overgrown with BCE in a 3-dimensional collagen gel (vitrogen-100, Collagen Corp., Fremont, CA, USA) as described by van der Schaft *et al.* (31). Following gelation, culture medium containing 20 ng/mL bFGF, with or without anginex or DBF analogs, was applied on top of the gel. After 24 hours of cell culture at 37 °C, photographs were made as

shown in the figure. The amount of sprouting in each well (i.e. the total length of the sprouts) was quantified by the computer program NIH image. To quantify differences in sprouting and tube formation, statistical analysis was performed using the Mann-Whitney U test.

Tumor model studies in athymic (nude) mice—In all studies, female athymic nude mice (nu/nu, 5-6 weeks old) were used. These mice were purchased from the National Cancer Institute and allowed to acclimatize to local conditions for at least one week. Animals were given water and standard chow *ad libitum*, and were kept on a 12 hour light/dark cycle. All experiments were approved by the University of Minnesota Research Animal Resources ethical committee. Mice were randomized and split into three groups: 1) human serum albumin (10 mg/kg/day), 2) anginex (10 mg/kg/day) and 3) DBF analog (10 mg/kg/day). Compounds were diluted in 100 mM SDS and administered using osmotic mini-pumps (Durect, Cupertino, CA). Exponentially growing MA148 human ovarian carcinoma cells, kindly provided by Prof. Ramakrishnan (18), were cultured in RPMI 1640 medium (Life Technologies, Grand Island, NY). This medium was supplemented with 10% fetal bovine serum and 1% penicillin/streptomycin (Cellgro, Mediatech, Washington, DC) at 37 °C and 5% CO_2. 100 μL of this tumor cell suspension (2×10^7 cells/ml) was then injected subcutaneously into the right flank of each mouse. Pumps were implanted into the left flank of mice for subcutaneous administration of compound over a 28-day treatment span.

Two variants of this model were used: prevention and intervention. For the prevention variant, treatment was initiated at the time of inoculation with MA148 cells. For the intervention variant, tumors were allowed to grow to an average size of 50 mm^3 (usually day 7 post inoculation) before treatment was initiated. With either variant, animals were randomized prior to the initiation of treatment. Treatment was administered via osmotic mini-pumps (Durect, Cupertino, CA), which were implanted subcutaneously in the left flank of mice. Concentrated solutions of anginex or DBF analogs were formulated such that the 28-day treatment period would be covered by implantation of a single pump. In each study, control groups of animals were administered either PBS or PBS containing human serum albumin. Tumor growth curves were found to be virtually identical in either of these control cases.

Tumor volume was determined by measuring the diameters of tumors using calipers (Scienceware, Pequannock, NJ) using the equation for the volume of a spheroid: $(a^2 \times b \times \Pi) / 6$, where 'a' is the width and 'b' the length of the tumor. Measurements were performed two or three times per week. At the conclusion of an experiment, tumor weights were also taken following excision of the tumors from euthanized animals. Tumor weights correlated well with tumor volumes calculated in this way.

Immunohistochemistry—Immunohistochemistry was used to assess microvessel density and the extent of total cell apoptosis. Tumor tissue was embedded in tissue freezing medium (Miles Inc, Elkart, IN) and shock frozen in liquid nitrogen. Sections of tissue (10 μm thickness) were prepared for immunohistochemical analysis. For this, tissue sections were brought to room temperature, air dried overnight, and then fixed in acetone for 10 minutes. Slides were allowed to air dry for at least 30 minutes and were washed three times for 5 minutes each in phosphate-buffered saline (PBS, pH 7.4). Samples were then blocked with PBS containing 0.1% bovine serum albumin and 3% human serum albumin for at least 30 minutes at room temperature in a humidified box. Samples were subsequently incubated with phycoerytrin (PE)-conjugated monoclonal antibody to CD31 (PECAM-1) in a 1:50 dilution (Pharmigen, San Diego, CA) to stain for microvessel density. After 1-hour incubation at room temperature, slides were washed with PBS and immediately imaged using an Olympus BX-60 fluorescence microscope at 200X magnification.

To assess the extent of total cell apoptosis, tissue sections were stained by using the TUNEL (terminal deoxyribonucleotidyl transferase-mediated dUTP-nick-end labeling) assay, which was performed according to the manufacturer's instructions (*in situ* cell death detection kit, fluorescein; TUNEL, Roche). Digital images were stored and processed using Adobe Photoshop (Adobe Inc., Mountain View CA). Quantification of microvessel density, the rate of proliferation and total cell apoptosis were determined as described earlier (32). Statistical analysis was performed using the Student's *t*-test.

Toxicity assays—As an indirect measurement of general toxicity, body weights of mice were monitored twice weekly, using a digital balance (Ohaus Florham, NJ). To determine hematocrit and creatinine levels, blood samples were extracted by tail vein bleedings one day after

terminating treatment and blood was collected in heparinized micro-hematocrit capillary tubes (Fisher; Pittsburgh, PA). For hematocrit levels, samples were spun down for 10 minutes in a micro-hematocrit centrifuge (Clay-Adams; NY), and the amount of hematocrit was determined using an international microcapillary reader (IEC; Needham, Mass). To obtain creatinine levels, a kit was purchased from Sigma (Sigma Diagnostics; St Louis, MO) and used according to the manufacturer's instructions.

RESULTS

Design of a partial-peptide mimetic—For input into designing the mimetic, we first performed structure-activity studies on anginex. Working with this relatively small peptide 33mer allowed for a thorough assessment of functionally-key residues by using alanine scanning and walk-through variants. The relative anti-proliferative effect of alanine-substituted analogs of anginex against EC is plotted in Figure 1*A*. Residues that demonstrate the most significant drop in the ability of anginex to inhibit EC proliferation are hydrophobic residues within the first two ß-strands: I3, L5, V7, L11 and I20. Conformationally, these functionally key hydrophobic residues all lie on the same face of the amphipathic anti-parallel ß-sheet (17,21). Also shown in Figure 1*A* are anti-proliferation activities of eight walk-through dodecapeptides that successively sample segments of the anginex sequence, shifting three residues in each peptide. Only three walk-through peptides (IC_{50} values listed at the right) demonstrate any significant anti-proliferative activity relative to parent anginex. As with results from alanine scanning, these peptides also encompass ß-strands 1 and 2. Based on these results, we concluded that antiangiogenic activity is localized within ß-strands 1 and 2 and that residues in turns 1 and 2 and ß-strand 3 are functionally dispensable. For orientation, the ß-strand alignment for anginex is depicted in Figure 1*B*; portions of the molecule containing the key sequences are boxed.

Using this information, we designed the DBF-series of partial-peptide mimetics, in which ß-strand 3 and turn 2 of anginex were omitted and a dibenzofuran (DBF) ß-turn mimetic (33,34) was used in place of turn 1 and residues F12, K13 and W18, K19 of ß-strands 1 and 2, respectively. The DBF ß-turn mimetic was used in order to maintain the bioactive ß-sheet conformation of anginex (21). The parent DBF-based compound depicted in Figure 1*C* is called 11DBF7, where numbers at the left and right of DBF refer to the number of amino acid residues

in the N- and C-terminal strands, respectively, from anginex. To identify the shortest sequences required for bioactivity, a series of N- and C-terminal deletion variants of 11DBF7 was made as listed in Table I.

ß-sheet structure is preserved in DBF analogs—We used NMR spectroscopy to investigate whether ß-sheet conformation was preserved in DBF analogs. Analogs 11DBF7 and 6DBF7 (that has more equivalent ß-strand lengths) were the focus of this structural study. Due to their limited water solubility and the desire to mimic a membrane-like environment, these compounds were investigated in dodecylphosphocholine (DPC) micelles. At the millimolar concentrations required for NMR work, 11DBF7 gave overlapping resonances that made spectral analysis ambiguous, whereas 6DBF7 gave excellent NMR spectra that allowed complete structure analysis. NOEs and coupling constants diagnostic of anti-parallel ß-sheet conformation were readily identified and used in computational modeling. The superimposed 28 lowest energy structures (Fig. 2*A*) have a backbone RMSD value (N- and C-terminal residues excluded) of 0.11 Å. Additional structural statistics are given in Table II. A simplified illustration of this folding pattern is shown in Figure 2B, which highlights residues on both hydrophobic and hydrophilic surfaces of the ß-sheet. In this orientation of the molecule, the dibenzofuran moiety is lying on edge. Notice also that two aliphatic hydrophobic residues leucine (L11) and isoleucine (I20) from anginex are packed against the phenyls of the DBF group in 6DBF7 (Fig. 2*B*). In effect, this sets up and helps to stabilize the ß-sheet fold (22). Based on this structural information, we concluded that other DBF analogs would fold similarly, albeit to various extents depending on the lengths of the two strands, i.e., strands of equal length are expected to be better able to form ß-sheets.

DBF analogs retain antiangiogenic activity—In endothelial cell (EC) proliferation assays, we demonstrated that 11DBF7, as well as a number of shorter analogs, including 6DBF7, are effective at inhibiting EC growth. Exemplary dose response curves for all xDBF7 analogs are given in Figure 3*A*, and IC_{50} values for all analogs are listed in Table I. Even though DBF analogs are less active than parent anginex, this may be explained in part by their having a decreased number of residues. Some of the analogs are missing residues identified by alanine scanning as being functionally important (e.g., L5 and I3). Nonetheless, a number of these

shorter analogs remain reasonably active, and it appears that the N-terminal hexapeptide SVQMKL and C-terminal hexapeptide IIVKLN are most essential for maintaining antiangiogenic activity.

Angiostatic potential was further demonstrated in the collagen gel-based sprout formation assay (21). Whereas control cultures show numerous sprouts (Fig. 3*B*), treatment with 6DBF7 (Fig. 3*C*), 11DBF7 (Fig. 3*D*) and anginex (Fig. 3*E*) all demonstrate highly reduced sprouting. These effects are quantified in Table 1. In general, reducing the number of amino acid residues in the ß-strands leads to reduced inhibition of sprout formation, comparable with results from the EC proliferation assay. Nonetheless, some analogs were active in this assay and one of the shortest analogs, 6DBF7, did demonstrate a significant inhibitory effect on tube formation. The kinetics of inhibition using DBF analogs, moreover, were the same as those observed with parent anginex (data not shown).

11DBF7 and 6DBF7 inhibit tumor growth in mice—Because our immediate interest in an antiangiogenic agent is in the area of tumor biology, we assessed the *in vivo* efficacy of two of the most *in vitro* active DBF analogs, 11DBF7 and 6DBF7, in the MA148 xenograft ovarian carcinoma tumor model in athymic mice (18-20). Our initial experiments using this model administered the parent analog, 11DBF7, subcutaneously via mini-pumps implanted at the time of inoculation with the tumor cell line. This prevention model demonstrated that treatment of tumor-bearing animals with 11DBF7 resulted in inhibition of tumor growth. Surprisingly, 11DBF7 functioned, on average, slightly better than anginex by reducing tumor volume by up to 80% relative to tumors from control animals (Fig. 4*A*).

In further experiments, we initiated treatment seven days after inoculation with tumor cells to allow establishment of tumors prior to the start of treatment. Using this protocol, anginex and 11DBF7, were found to inhibit tumor growth by up to 70% during the course of treatment (Fig. 4*B*). At the end of the four week administration period (day 35), the rate of tumor growth began to increase, but remained at about 50% ten days post-treatment (not shown) when animals were sacrificed for analysis of tumor tissue. Interestingly, the smaller analog, 6DBF7, was even more effective than anginex or 11DBF7 at inhibiting the growth of tumors (Fig. 4*B*). The reason for this is unclear, but may be related to improved bioavailability of 6DBF7.

Antiangiogenic potential *in vivo* was demonstrated immunohistochemically by staining tumor cross-sections from treated animals with fluorescently-labeled anti-CD31 antibody to identify blood vessels. As shown in Figures 4*C-F* and quantified in Table III, vessel density, relative to control (Fig. 4*C*), was significantly reduced by treatment with anginex (Fig. 4*D*), 11DBF7 (Fig. 4*E*) or 6DBF7 (Fig. 4*F*). These antiangiogenic compounds had a significant effect as well on vessel architecture, demonstrating a drop in the number of end points, branch points and vessel length (Table III). In addition, antiangiogenic treatment also reduced the rate of proliferation of tumor cells as determined by immunohistochemical staining of PCNA in cryosections of tumors (Table III). As a result of angiogenic inhibition, the number of apoptotic tumor cells increased from 311±103 in the control, to 620 ± 146 and 851 ± 162 in anginex and 6DBF7 treated animals, respectively.

In all *in vivo* experiments, treatment with anginex, 11DBF7 and 6DBF7 did not show any sign of toxicity as assessed by unaltered behavior and normal weight gain during experiments (see inserts to Fig. 4*A*, *B*). Moreover, hematocrit and creatinine levels in treated animals were normal relative to control, indicating the absence of toxicity to bone marrow and kidney, respectively. Upon autopsy, macro- and microscopic morphology of internal organs were also observed to be normal within all experimental groups of animals.

DISCUSSION

Here, we identified functionally key amino acid residues in the ß-sheet-forming anginex peptide that promote its angiostatic activity and using this SAR information, designed partial non-peptidic ß-sheet mimetics of anginex. Members of this novel class of DBF-based compounds are effective antiangiogenic agents both *in vitro* and *in vivo*. Moreover, the *in vivo* anti-tumor activity of one of these DBF mimetics, 6DBF7, is improved over that of the larger parent molecule anginex.

The ß-sheet conformation in particular is crucial to the antiangiogenic activity of these DBF analogs, just as it is for parent anginex peptide (17,21). 6DBF7 is shown here to fold as an amphipathic ß-sheet, with functionally key hydrophobic residues lying on the same face of the molecule. Interestingly, the crystal structure of VEGF complexed with an antiangiogenic peptide (Flt-1D2) (35) derived from one of its endothelial cell-specific tyrosine kinase receptors,

Flt-1, indicates that functionally key segments of Flt-1D2 are located within its ß-sheet domain. Moreover, one of the peptides derived from this domain, NITVTLKKFPL, inhibits angiogenesis through a non-VEGF binding mechanism, i.e., without binding to VEGF or inhibiting VEGF's binding to its receptors (36). CD and NMR analyses indicate that this Flt-1 peptide 11mer forms a stable extended ß-strand structure in solution. In this conformation, the peptide would present N-terminal hydrophobic amino acid residues I-V-L on the same face of the strand. This I-V-L presentation pattern is also present in 6DBF7 (ß-strand 2), along with the cross-strand hydrophobic pattern V-M-L (ß-strand 1). Although the efficacy of the Flt-1 peptide is much less than that of 6DBF7, this structural/compositional similarity between these two peptides suggests that on the molecular level, the ß-sheet structure of these molecules is pivotal to their activity (37) which may suggest signaling through a common cellular receptor.

Many other antiangiogenic proteins whose high-resolution molecular structures are known, e.gs., endostatin (14), PF4 (15), TNF-α (38), BPI (16), and TSP-1 type 1 repeat (39), are also structurally (antiparallel ß-sheet) and compositionally (high incidence of hydrophobic and positively charged residues) similar to anginex and DBF mimetics. Although this observation may indicate an evolutionary structural link among a number of antiangiogenic proteins, the meaning of this commonality remains unclear because their mechanisms of action and cellular receptors could be different. To complicate matters further, few receptors reported to mediate the signal leading to angiostasis are definitive and a number of antiangiogenic agents apparently can act on multiple receptors. For angiostatin, for example, three receptors on endothelial cells have been reported: ATP-synthase (40) and integrins $\alpha_v\beta_3$ and $\alpha_9\beta_1$(41). For endostatin, there are currently also at least three possibilities: a low affinity cell surface glypican receptor, along with a yet-to-be-identified high affinity receptor (42) and an intercellular epitope (hTM3) in tropomyosin (43). And for another well-known antiangiogenic protein, TSP-1, there are four identified receptors: syndecan, heparin sulfate proteoglycans (HSPG), integrin-associated protein (IAP) (reviewed in (12)) and its long-known transmembrane receptor CD36 (44,45).

Even with these uncertainities, the compositional and structural similarity noted among anginex, 6DBF7 and various antiangiogenic proteins and peptides may be used to further improve or optimize the efficacy of anginex peptide mimetics and in the design of additional novel therapeutic antiangiogenic agents. For the present, 6DBF7 appears to be one of the most potent antiangiogenic and antitumor agents known. This claim is supported by the observation

that anginex is as potent as angiostatin and more potent than endostatin at inhibiting the growth of ovarian tumors in mice (18). Therefore, based on the present comparison with anginex, 6DBF7 must also be more potent *in vivo* than endostatin or angiostatin. The design of 6DBF7 places us on the road to creating an actual small molecule pharmaceutical agent that could be used as an effective therapeutic against cancer, as well as against other angiogenically-related pathologic disorders like arthritis, restenosis, endometriosis and diabetic retinopathy.

Acknowledgements—This work was supported by research grants from the US National Cancer Institute (R01 CA- 96090 and CA-76497; to K.H.M.) and the Dutch Cancer Society (UM2001-2529; to A.W.G.).

Footnotes

Abbreviations: DBF, dibenzofuran; EC, endothelial cell; HUVEC, human umbilical vein EC; PBS, phosphate buffered saline; HPLC, high performance liquid chromatography; bFGF, basic fibroblast growth factor; VEGF, vascular endothelial growth factor; IL-8, interleukin-8; PF4, platelet factor-4; BPI, bactericidal-permeability increasing protein; NMR, nuclear magnetic resonance.

*Griffioen *et al.*. Unpublished data.

References

1. Griffioen, A. W., van der Schaft, D. W., Barendsz-Janson, A. F., Cox, A., Struijker Boudier, H. A., Hillen, H. F., and Mayo, K. H. (2001) *Biochem J* **354,** 233-42
2. O'Reilly, M. S., Boehm, T., Shing, Y., Fukai, N., Vasios, G., Lane, W. S., Flynn, E., Birkhead, J. R., Olsen, B. R., and Folkman, J. (1997) *Cell* **88,** 277-85
3. Boehm, T., Folkman, J., Browder, T., and O'Reilly, M. S. (1997) *Nature* **390,** 404-7
4. Molema, G., and Griffioen, A. W. (1998) *Immunol Today* **19,** 392-4.
5. Folkman, J. (1995) *Nat Med* **1,** 27-31
6. Gupta, S. K., and Singh, J. P. (1994) *J Cell Biol* **127,** 1121-7
7. Tolsma, S. S., Volpert, O. V., Good, D. J., Frazier, W. A., Polverini, P. J., and Bouck, N. (1993) *J Cell Biol* **122,** 497-511
8. Luster, A. D., Greenberg, S. M., and Leder, P. (1995) *J Exp Med* **182,** 219-31
9. O'Reilly, M. S., Holmgren, L., Shing, Y., Chen, C., Rosenthal, R. A., Moses, M., Lane, W. S., Cao, Y., Sage, E. H., and Folkman, J. (1994) *Cell* **79,** 315-28
10. Ramchandran, R., Dhanabal, M., Volk, R., Waterman, M. J., Segal, M., Lu, H., Knebelmann, B., and Sukhatme, V. P. (1999) *Biochem Biophys Res Commun* **255,** 735-9
11. van der Schaft, D. W., Toebes, E. A., Haseman, J. R., Mayo, K. H., and Griffioen, A. W. (2000) *Blood* **96,** 176-81
12. Chen, H., Herndon, M. E., and Lawler, J. (2000) *Matrix Biol* **19,** 597-614
13. Dings, R. P. M., Nesmelova, I., Griffioen, A. W., and Mayo, K. H. (2003) *Angiogenesis in press*
14. Hohenester, E., Sasaki, T., Olsen, B. R., and Timpl, R. (1998) *EMBO J* **17,** 1656-1664
15. Mayo, K. H., Roongta, V., Ilyina, E., Milius, R., Barker, S., Quinlan, C., La Rosa, G., and Daly, T. J. (1995) *Biochemistry* **34,** 11399-11409
16. Beamer, L. J., Carroll, S. F., and Eisenberg, D. (1997) *Science* **276,** 1861-1864
17. Mayo, K. H., van der Schaft, D. W., and Griffioen, A. W. (2001) *Angiogenesis* **4,** 45-51
18. Dings, R. P., Yokoyama, Y., Ramakrishnan, S., Griffioen, A. W., and Mayo, K. H. (2003) *Cancer Res* **63,** 382-5
19. Dings, R. P., van der Schaft, D. W., Hargittai, B., Haseman, J., Griffioen, A. W., and Mayo, K. H. (2003) *Cancer Lett* **194,** 55-66
20. van der Schaft, D. W., Dings, R. P., de Lussanet, Q. G., van Eijk, L. I., Nap, A. W., Beets-Tan, R. G., Bouma-Ter Steege, J. C., Wagstaff, J., Mayo, K. H., and Griffioen, A. W. (2002) *Faseb J* **16,** 1991-1993
21. Dings, R. P., Arroyo, M. M., Lockwood, N. A., Van Eijk, L. I., Haseman, J. R., Griffioen, A. W., and Mayo, K. H. (2003) *Biochem J* **23,** 281-288
22. Bekele, H., Nesloney, C. L., McWilliams, K. W., Zacharias, N. M., Chitnumsub, P., and Kelly, J. W. (1997) *J Org Chem* **62,** 2259-2262
23. Carpino, L. A. (1993) *J. Am. Chem. Soc.* **115,** 4397-4398
24. King, D. S., Fields, C. G., and Fields, G. B. (1990) *Int J Pept Protein Res* **36,** 255-66.
25. Piotto, M., Saudek, V., and Sklenar, V. (1992) *J Biomol NMR* **2,** 661-5
26. Wider, G., Macura, S., Anil-Kumar, Ernst, R. R., and Wüthrich, K. (1985) *J. Magn. Reson.* **56,** 207-234
27. Shaka, A. J., Lee, C. J., and Pines, A. (1988) *J. Magn. Reson.* 77, 274-293
28. Rucker, S. P., and Shaka, A. J. (1989) *Mol. Phys.* **68,** 509-517
29. Delaglio, F., Grzesiek, S., Vuister, G. W., Zhu, G., Pfeifer, J., and Bax, A. (1995) *J Biomol NMR* **6,** 277-93

30. Brunger, A. T. (1992) *X-plor Manual*, Yale University Press, New Haven
31. van der Schaft, D. W., Wagstaff, J., Mayo, K. H., and Griffioen, A. W. (2002) *Ann Med* **34,** 19-27
32. Wild, R., Ramakrishnan, S., Sedgewick, J., and Griffioen, A. W. (2000) *Microvasc Res* **59,** 368-76
33. Diaz, H., Tsang, K. Y., D., C., J.R., E., and J.W., K. (1993) *J. Am. Chem. Soc.* **115,** 3790-3791
34. Tsang, K. Y., Diaz, H., Graciani, N., and Kelly, J. W. (1994) *J. Am. Chem. Soc.* **116,** 3988-4005
35. Wiesmann, C., Fuh, G., Christinger, H. W., Eigenbrot, C., Wells, J. A., and de Vos, A. M. (1997) *Cell* **91,** 695-704
36. Tan, D. C., Kini, R. M., Jois, S. D., Lim, D. K., Xin, L., and Ge, R. (2001) *FEBS Lett* **494,** 150-6
37. Kranenburg, O., Bouma, B., Kroon-Batenburg, L. M., Reijerkerk, A., Wu, Y. P., Voest, E. E., and Gebbink, M. F. (2002) *Curr Biol* **12,** 1833-9
38. Jones, E. Y., Stuart, D. I., and Walker, N. P. (1989) *Nature* **338,** 225-228
39. Tan, K., Duquette, M., Liu, J. H., Dong, Y., Zhang, R., Joachimiak, A., Lawler, J., and Wang, J. H. (2002) *J Cell Biol* **159,** 373-82
40. Moser, T. L., Stack, M. S., Asplin, I., Enghild, J. J., Hojrup, P., Everitt, L., Hubchak, S., Schnaper, H. W., and Pizzo, S. V. (1999) *Proc Natl Acad Sci U S A* **96,** 2811-2816
41. Tarui, T., Miles, L. A., and Takada, Y. (2001) *J Biol Chem* **276,** 39562-8
42. Karumanchi, S. A., Jha, V., Ramchandran, R., Karihaloo, A., Tsiokas, L., Chan, B., Dhanabal, M., Hanai, J. I., Venkataraman, G., Shriver, Z., Keiser, N., Kalluri, R., Zeng, H., Mukhopadhyay, D., Chen, R. L., Lander, A. D., Hagihara, K., Yamaguchi, Y., Sasisekharan, R., Cantley, L., and Sukhatme, V. P. (2001) *Mol Cell* **7,** 811-822
43. MacDonald, N. J., Shivers, W. Y., Narum, D. L., Plum, S. M., Wingard, J. N., Fuhrmann, S. R., Liang, H., Holland-Linn, J., Chen, D. H., and Sim, B. K. (2001) *J Biol Chem* **276,** 25190-25196
44. Dawson, D. W., Pearce, S. F., Zhong, R., Silverstein, R. L., Frazier, W. A., and Bouck, N. P. (1997) *J Cell Biol* **138,** 707-717
45. Jimenez, B., Volpert, O. V., Crawford, S. E., Febbraio, M., Silverstein, R. L., and Bouck, N. P. (2000) *Nat Med* **6,** 41-8

Table I

N- and C-terminal deletion variants of 11DBF7 and angiostatic potential

	Amino Acid Sequence	EC Proliferation (IC50)	% Sprouting[a]
Anginex	parent peptide 33mer	3 μM	8 ± 5%*
DBF Analogs			
11DBF7	ANIKLSVQMKL-[DBF]-IIVKLND	12 μM	23 ± 10%[b]
10DBF7	NIKLSVQMKL-[DBF]-IIVKLND	12 μM	57 ± 17%[b]
9DBF7	IKLSVQMKL-[DBF]-IIVKLND	20 μM	76 ± 40%
6DBF7	SVQMKL-[DBF]-IIVKLND	15 μM	60 ± 12%[b]
4DBF7	QMKL-[DBF]-IIVKLND	25 μM	99 ± 5%
3DBF7	MKL-[DBF]-IIVKLND	>>[c]	84 ± 30%
1DBF7	L-[DBF]-IIVKLND	>>[c]	>>[c]
11DBF6	ANIKLSVQMKL-[DBF]-IIVKLN	22 μM	115 ± 7.4%
11DBF4	ANIKLSVQMKL-[DBF]-IIVK	35 μM	115 ± 16.3%
11DBF1	ANIKLSVQMKL-[DBF]-I	23 μM	114 ± 13.6%
6DBF6	SVQMKL-[DBF]-IIVKLN	42 μM	96.8 ± 2.7%
6DBF4	SVQMKL-[DBF]-IIVK	>>[c]	80.4 ± 0.3%
6DBF3	SVQMKL-[DBF]-IIV	>>[c]	80.0 ± 17.4%
6DBF2	SVQMKL-[DBF]-II	>>[c]	118 ± 15.8%
6DBF1	SVQMKL-[DBF]-I	76 μM	111 ± 13.6%

[a] Significant inhibition ($P < 0.03$; Mann-Whitney U test).
[b] Relative to control culture with medium alone.
[c] The compound had no effect on the assay.

Table II

Structural statistics for NOE-derived structures of 6DBF7

RMS Deviations from experimental distance restraints (Å)[a]	
NOE (168)	0.1 ± 0.01
H-bond (16)	
Deviations from idealized geometry	
Bonds (Å)	0.0071 ± 0.0004
Angles (°)	1.0 ± 0.03
Impropers (°)	0.6 ± 0.05
Energies ($kcal.mol^{-1}$)	
E_{NOE}[b]	89.9 ± 10.5
E_{BOND}	13.2 ± 1.4
E_{ANGLE}	71.8 ± 4.2
$E_{IMPROPER}$	7.4 ± 1.3
E_{TOTAL}	202.6 ± 22.4

[a] None of the 28 final structures exhibited distance restraint violations greater than 0.5 Å or dihedral angle violations greater than 5°. RMSD values represent the mean and standard deviations for the 28 structures.

[b] The final value of the NOE (E_{NOE}) was calculated with a force constant of 50 $kcal.mol^{-1}.Å^{-2}$.

Table III

Microvessel density and proliferation rate in tumors of treated mice

	Proliferation[a]	Vessel Density[b]	End Points[c]	Branch Points[d]	Vessel Length[e]
Vehicle	848 ± 104	5858 ± 656	26.2 ± 2.2	7.6 ± 1.4	5.9 ± 0.7
Anginex	414 ± 44	2245 ± 329	22.9 ± 2.2	2.1 ± 0.6	0.9 ± 0.3
11DBF7	553 ± 75	2879 ± 385	21.2 ± 3.3	3.1 ± 0.9	3.0 ± 0.6
6DBF7	501 ± 68	2213 ± 256	21.7 ± 2.6	2.3 ± 1.1	2.5 ± 0.4

[a]After binarization of the images of the PCNA-staining, proliferation was estimated by scoring the total number of white pixels per field.

[b]After binarization of the images of the CD31-staining, microvessel density was estimated by scoring the total number of white pixels per field.

[c]Mean number of vessel end points as determined after skeletonization of the images (32).

[d]Mean number of vessel branch points/nodes per image.

[e]Mean total vessel length per image.

All results are expressed as mean pixel counts per image (± standard error).

Figure legends

Fig. 1. **Effects of alanine scan and walk-through variants of anginex on EC proliferation *in vitro*.** The sequence is shown for anginex in single letter codes of amino acid residues, below which are given the amino acid sequences for the dodecapeptide walk-throughs of anginex (*panel A*). Proliferation of bFGF-stimulated (10 ng/ml) human umbilical vascular EC (HUVEC) cultures was measured by quantification of ^{3}H-thymidine incorporation. Proliferation is expressed as mean counts per minute (cpm) of quadruplicate cultures in three independent experiments (± SEM). EC proliferation results from alanine scanning (tested at 25 μM dose) are expressed in bar graph format as the percentage of proliferating EC {the arithmetic mean cpm of triplicate cultures} relative to control cultures (no inhibitor). For walk-through peptides, results are given as IC_{50} values from dose response curves; only IC_{50} values for dodecapeptides with significant activity relative to anginex are given. The overall fold for anginex (3 ß-strands with 2 turns) is shown with functionally key residues boxed (*panel B*). The parent DBF analog is depicted with the introduction of the scaffold and the two functionally key ß-strand sequences from anginex (*panel C*).

Fig. 2. **The superposition of 28 structures of 6DBF7 derived from NMR analysis and the chemical 3D structure representation of 6DBF7.** The dibenzofuran moiety is shown head-on at the top right of the structures (*panel A*). Polar residues on the hydrophilic side of the amphipathic ß-sheet of 6DBF7 are highlighted with squares, whereas non-polar residues on the hydrophobic side of the amphipathic ß-sheet of 6DBF7 are highlighted with circles (*panel B*).

Fig. 3. **Bioactivity of DBF analogs in *in vitro* assays.** The anti-proliferative effects of some DBF analogs on bFGF-activated EC are plotted as dose response curves (*panel A*). To assess antiangiogenic potential of these DBF analogs, sprouting and tube formation were studied using cytodex-3 beads overgrown with BCE in a 3-dimensional collagen gel. Tube formation experiments under control conditions (*panel B*), or in the presence of 6DBF7 (*panel C*), 11DBF7 (*panel D*) or anginex (*panel E*), at a concentration of 25 μM are shown. The beads have a mean size of 170 (± 40) microns.

Fig. 4. **6DBF7 inhibits tumor growth in mice.** MA148 tumor bearing mice were treated with the optimal dose of anginex (10 mg/kg/day) or equivalent doses of 11DBF7 or 6DBF7. Treatment was initiated at the time of inoculation with MA148 cells (*panel A*). An intervention study is shown where tumors were allowed to establish to a palpable size before treatment was initiated (*panel B*). In either study, control groups of animals were treated with PBS containing human serum albumin to control for protein content. Tumor volumes (*panels A and B;* for all groups n=11, ± SEM) are plotted as mm^3 vs. days post inoculation. The inserts show the body weight development of the mice during the study as a measurement of overall toxicity. Immunohistochemical analysis of microvessel density is shown (*panels C through F*). *C* represents the average amount of microvessels in the tumor of a control treated animal. *Panels D, E,* and *F* represent the average amount of vessel density staining on tumor tissue from anginex-, 11DBF7- and 6DBF7-treated animals, respectively. Original magnification X200; scale bar = 50 μm.

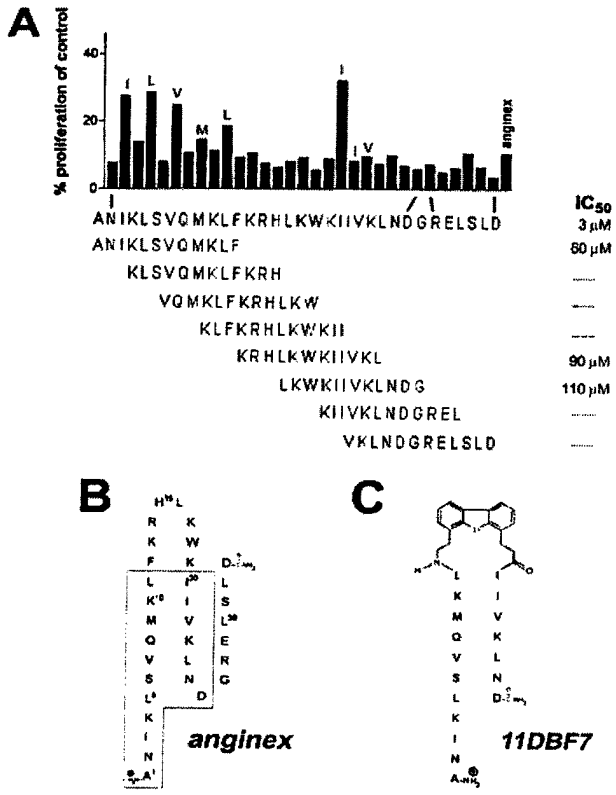

Figure 1,
Mayo et al

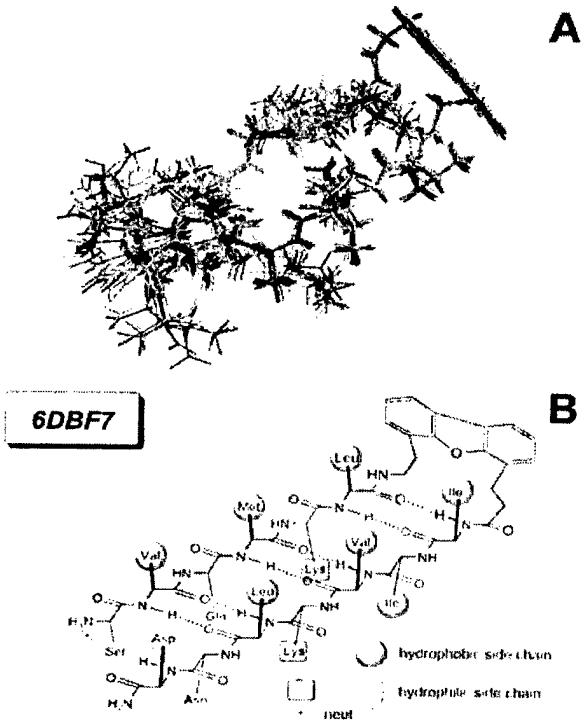

Figure 2,
Mayo et al

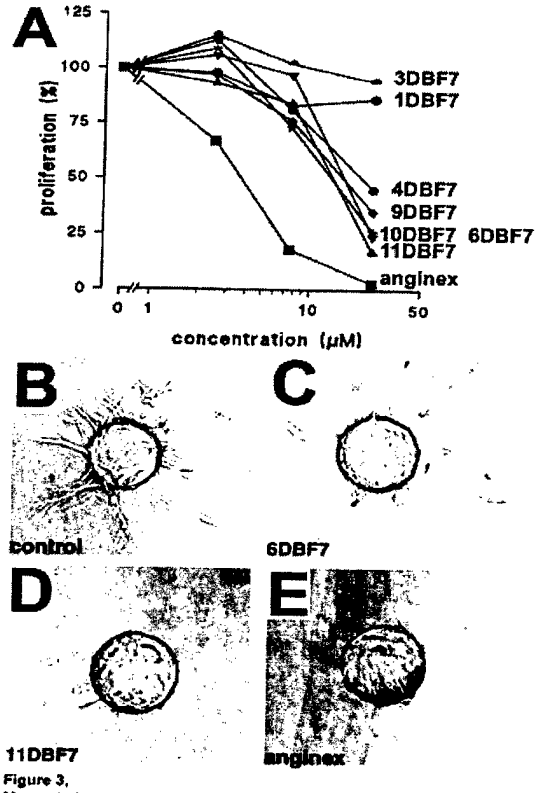

Figure 3,
Mayo et al

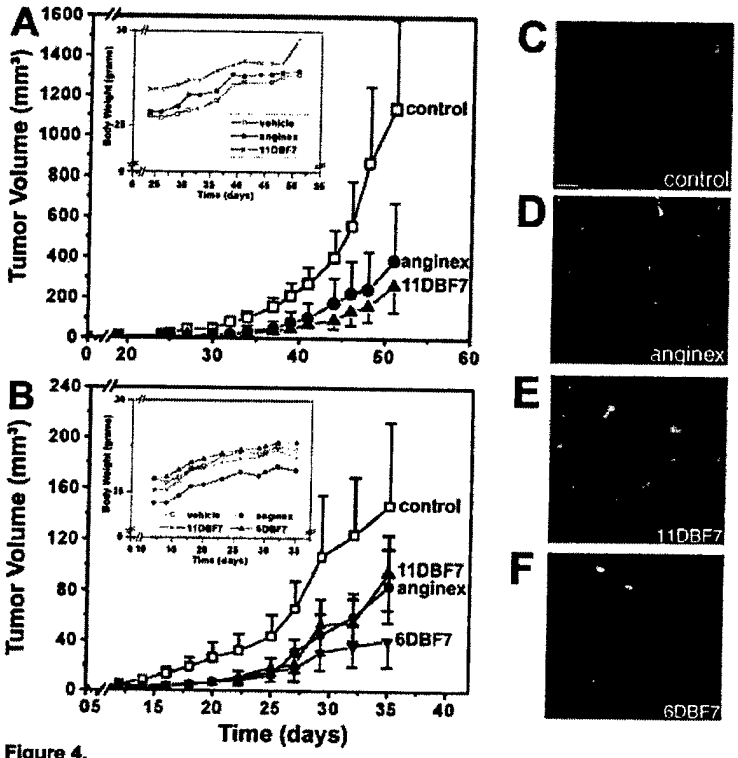

Figure 4,
Mayo et al